Title
An Analysis of Wideband Beamforming Techniques and Hardware Requirements for Analog and Digital Radar Architectures

Author
Singh, Jasmin

Publication Date
2021

Peer reviewed|Thesis/dissertation

UNIVERSITY OF CALIFORNIA

Los Angeles

An Analysis of Wideband Beamforming Techniques and Hardware Requirements for Analog and Digital Radar Architectures

A thesis submitted in partial satisfaction

of the requirements for the degree

Master of Science in Electrical and Computer Engineering

by

Jasmin Singh

2021

ABSTRACT OF THE THESIS

An Analysis of Wideband Beamforming
Techniques and Hardware Requirements
for Analog and Digital Radar Architectures

by

Jasmin Singh
Master of Science in Electrical and Computer Engineering
University of California, Los Angeles, 2021
Professor Danijela Cabric, Chair

Due to the growing complexity and increased capability of radar systems, various enhancements to the design and testing of radars need to be considered. This project will focus on the understanding of implementations of analog, hybrid, and fully-digital radar architectures such as phased antenna arrays, antenna subarrays, and digital MIMO arrays. In addition, the project will include the evaluation of the performance of various established wideband beamforming algorithms in terms of their capabilities in nulling and frequency invariance in the presence of nonlinearities, caused by the use of wideband signals. This will also include implementations of several algorithms and evaluations of the effects of finite precision due to the limited resolutions of ADCs and phase shifters.

The thesis of Jasmin Singh is approved.

Yuanxun Ethan Wang

Greg Pottie

Danijela Cabric, Committee Chair

University of California, Los Angeles

2021

TABLE OF CONTENTS

List of Figures

List of Tables

ACKNOWLEDGMENTS

This research was conducted in volatile times of the pandemic and encountered several speed bumps along the way. Before I started my graduate degree, I would have never have predicted the events that occurred in the past two years in which I slowly and steadily completed this thesis. Although this experience was not ideal, I am truly grateful that I was able to come this far.

The difficulties experienced during this time were ameliorated with the help of my advisor, Professor Danijela Cabric. I would like to express my gratitude to her for taking the time out to help me along this process. I would also like to thank my mentors, as well as my thesis committee members for giving me valuable feedback on my thesis.

Lastly, I would like thank my Mom, Dad, Sister, and my dog, Bear, who have provided me with love and support. Although life with them is crazy at times, their presence helps me to keep progressing.

CHAPTER 1

Background

Radar technology has been used for decades as a reliable tool for gathering information such as distance, direction, position, and imaging. This information helps to strengthen defense operations, space exploration, climate and agriculture, and more recently, the automotive industry with autonomous vehicles. Radars have relied on phased-antenna array systems but are moving towards more digital architectures such as multiple-input multiple-output (MIMO) antenna arrays. Phased-array systems are well-studied and offer better commercial access to components, making them easier to manufacture. Digital architectures come with enhanced capabilities and smaller packaging, but with the possibility of increased cost. One important distinction between the analog and digital architectures is their handling of wideband communication.

The advancement in radar applications warrants the use of wideband and ultra-wideband to render advanced capabilities to be useful. The wider bandwidth, as opposed to traditional narrowband signals, offer finer resolution. The spatial signal processing or beamforming helps to process radar data into useful information. Beamforming algorithms were designed based on narrow-band signals and have limitations for wideband signals. One major issue with radar systems is the handling of beam squinting or frequency invariance that comes with the use wider frequency bands. When the beampattern is not desired over the frequency bandwidth, the locations where specific nulling and high gain is required will suffer. This could prevent from meeting requirements of the radar system being designed. This section will aim to go over basic radar concepts as they relate to beampattern formation, examples

of analog, digital, and hybrid radar antenna architectures such as phased-antenna, MIMO, and phased-MIMO arrays, as well as the distinction between the hardware in analog and digital radar implementations. This information will help setup the problems and important considerations associated with wideband radars.

1.1 Radar and Antenna System Overview

The general radar transmission and reception process begins with a transmitter which utilizes antenna systems via the transmit/receive (T/R) device, to propagate electromagnetic waves. The reflection of the signal including reflections from the target and clutter are collected at the radar receiver. The received signal is then typically amplified, converted from RF to an intermediate frequency (IF), converted from analog to digital, and then enters a signal processor. The received signal typically contains interference from internal/external electronic noise, clutter, electromagnetic interference, and electronic counter measures (ECM) in the form of noise or false targets [1]. This general model is illustrated in figure 1.1. The radar

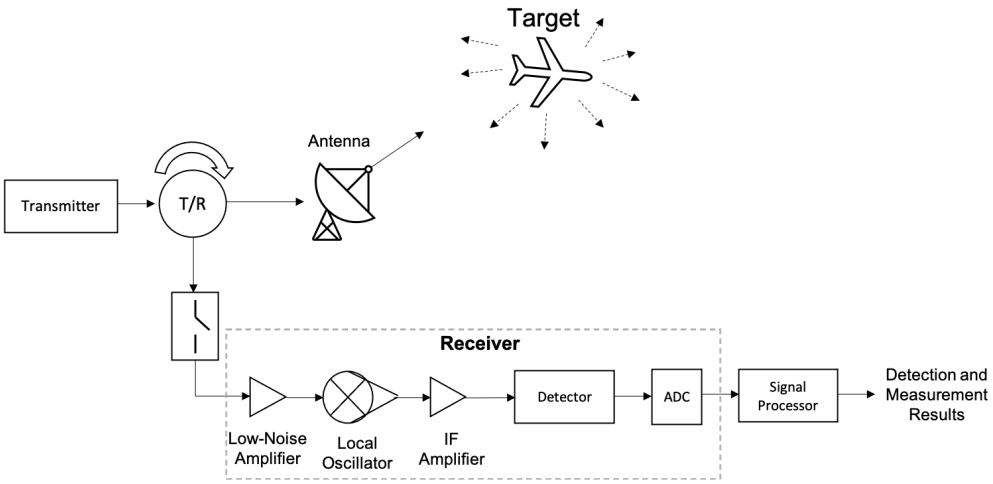

Figure 1.1: General radar transmission and reception process [1].

range equation, R, is expressed as

$$R_{max} = \left[\frac{P_t G_t G_r \lambda^2 \sigma}{(4\pi)^3 L_s P_{min}} \right]^{1/4} \tag{1.1}$$

where P_t is the transmit power, G_t is the transmit gain, G_r is the receive gain, λ is the carrier wavelength, σ is the radar cross-section of the target, L_s is combined losses, and P_{min} is the minimum detectable signal power. The minimum resolvable range for a compressed waveform is

$$\Delta R = \frac{c}{2BW} \tag{1.2}$$

where c is the speed of light constant and BW is the radar's instantaneous bandwidth in Hz which is limited by the antenna. The antenna system is vital to the performance of the radar. It acts as the radars eyes, meaning only objects in its field-of-view (FOV) can be detected. The radar antenna converts transmission line propagation into free-space propagation and vice versa. There are various antenna characteristics that define its performance and its suitable use. Antennas are desired to have narrow beam widths in order to have accurate angular resolution so targets that are close together can be easily resolved [3]. Generally, power and aperture can often be traded to achieve the desired performance. If the antenna was built to have a small aperture, the power can be increased and vice versa.

An isotropic antenna is an ideal point source that transmits and receives energy equally in all directions. The intensity in watts/steradian and power density in W/m^2 is formulated as

$$I = \frac{P_t}{4\pi} \tag{1.3}$$

$$Q_t = \frac{P_t}{4\pi R^2} \tag{1.4}$$

where P_t is the total power radiated by the antenna, 4π is the steradian area of the sphere, and R is the distance from the center of the antenna. Each concentric circle outside the antenna has its own intensity and phase which is ideally constant throughout that circular plane.

In actuality, the radiated energy from an antenna is dependent on the angle. For a linear array of isotropic antennas, the summation point is the location where the individual element signals combine. The plane wave has the property that everywhere perpendicular to the direction of propagation, the electric field is in phase. At $\theta = 0°$, the antennas will detect the same phase, however at different angle, each antenna element will detect a different phase from the plane wave due to the time delay associated with each antenna's position. The energy at the summation point will not be coherent and destructive interference can result in lost of receipt energy [1].

Equation 1.1 shows radars achieve better resolution and signal-to-noise ratio when the antenna gain is large since it directly impacts the received echo signal. There are two types of gain that are related to each other: directive gain and power gain. The directivity gain describes the antenna pattern whereas the power gain includes both antenna pattern descriptions and dissipative losses. Power gain is the gain term used in the radar equation. Gain is often represented as a normalized function of angle of propagation, where it is referred to as relative gain. Aperture efficiency (ρ_a) is the measure of effective area (A_e) presented by the antenna to the incident wave. Gain can be formulated in terms of the effective aperture as

$$G = \frac{4\pi A_e}{\lambda^2} = \frac{4\pi \rho_a A}{\lambda^2} \tag{1.5}$$

where A is the physical area of the antenna. The aperture is most efficient when uniformly illuminated which is realized when $\rho_a = 1$. Thus, the maximum directivity for a uniformly illuminated antenna is

$$G_{max} = \frac{4\pi(0.88)^2}{\theta_B \phi_B} \tag{1.6}$$

where θ_B and ϕ_B are half-power bandwidths in units of radians for the two principal planes, azimuth and elevation. Aperture is the phase variation across the array surface and can be defined as

$$\Delta\phi = \frac{2\pi L \sin\theta}{\lambda} \tag{1.7}$$

where L is the length of the antenna and can be replaced by $n\Delta x$ for an array of antenna elements. The n is the number of antenna elements in the array and Δx is the distance between each element. We can deduce that as aperture increases, the antenna response will change at a higher rate with respect to θ. The beam width of an antenna is inversely proportional to its size and can be expressed in radians as

$$\theta_B = \frac{\alpha\lambda}{L} \tag{1.8}$$

where α is the beam width factor inherent to the antenna and determined by the aperture taper function and aperture shape. If the aperture is circular and uniformly weighted, α is approximately 1 [1].

Sidelobe radiation refers to the curves in the beam pattern aside from the main lobe. Ideally, sidelobes should be minimized so that energy is directed toward the main beam. Large sidelobes can cause false detections and make the radar more susceptible to jamming and other interferences. The average sidelobe is often a metric to characterize the sidelobe return. The average ratio of the sidelobe power to that of an isotropic antenna with the same input power is

$$SL_{ave} = \frac{\frac{P_{SL}}{\Omega_{SL}}}{\frac{P_t}{4\pi}} \approx 1 - \frac{P_{MB}}{P_t} \tag{1.9}$$

where P_{SL} is the power radiated into the sidelobe, P_{MB} is the power radiated into the main beam, and Ω_{SL} is the steradian area of the sidelobe. The average sidelobe level must be below isotropic or 0 dBi [1]. Sidelobes can be reduced using windows or tapers. Commonly used windows include Hamming, Hanning, Blackman, and Kaiser. Windowing allows the power to be concentrated at the center at the expense of widening the main beam, creating a tradeoff [4]. An example of the Hamming window for 10 and 20 antennas is shown in figures 1.2 and 1.3. Similar to the opening for a camera lens, the aperture is the radiating surface of an antenna or the opening in a plane directly in front of the antenna through which all the power radiated or received by the antenna passes. The electrical field distribution is called the aperture taper. If the taper is uniform, the antenna will have the greatest directivity

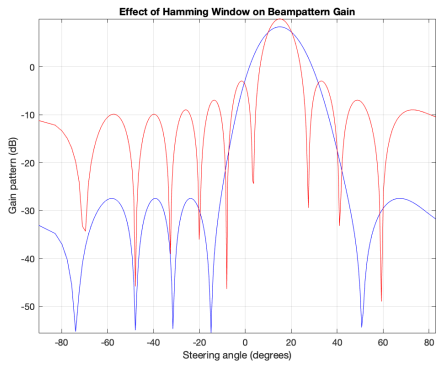

Figure 1.2: Baseline beampattern (red) and windowing effect (blue) with 10 elements.

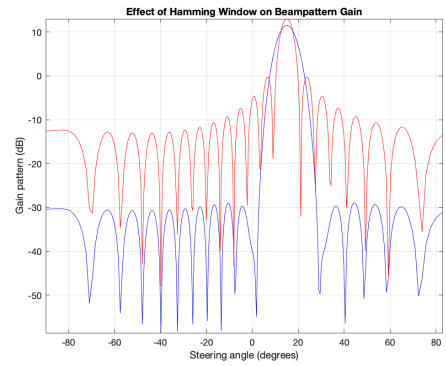

Figure 1.3: Baseline beampattern (red) and windowing effect (blue) with 20 elements.

and narrowest beam width possible, however, the resulting sidelobes will be large. The peak sidelobe can be reduced by tapering, but this will reduce the power in the main beam, thus creating a tradeoff between maximizing directivity and decreasing the sidelobe level. Various tapers can be used, a popular option being the Taylor function. In actuality, the function used is never perfect due to the differences in a real antenna system including thermal effects, tolerances, alignment, etc. These factors cause taper errors which are random deviations in amplitude and phase from the ideal taper function. Phase errors are typically harder to control and more destructive than amplitude errors [1].

1.2 Phased-Array, MIMO, and Phased-MIMO Antenna Systems

1.2.1 Analog Radar Architecture: Phased Antenna Array

Phased array or electronically steered antenna systems are commonly used in modern military systems. They brought higher reliability, larger bandwidth, and better sidelobe control than the preceding antenna technology. Phased array antennas allow for quiet operation since there is no physical rotation. They are also faster than the mechanically steered antenna.

In a traditional uniform linear array, the Array Factor (AF) is the sum of the individual element voltage responses normalized by the number of elements N. This is expressed as

$$AF(\theta) = \frac{1}{N}\sum_{n=1}^{N} \exp[-j(\frac{2\pi}{\lambda} n\Delta x \sin\theta - \phi_n)] \tag{1.10}$$

where Δx is the antenna spacing and ϕ_n is the relative phase shift between the nth element and the array summation point. The total radiation pattern of a phased array is the product of the array factor and the individual element pattern. If the antenna is isotropic, the array factor and phased array radiation pattern will be equal. If the path length from each element to the summation point is equal, in other words, when $\theta = 0°$, or if $\phi_n = 0°$ for all n, the AF will be at its maximum when the plane wave approaches from a direction normal to the array. The element signals will no longer have equal phases when the angle increases [1]. This is shown in figure 1.4. When the nth element is excited by a plane wave arriving

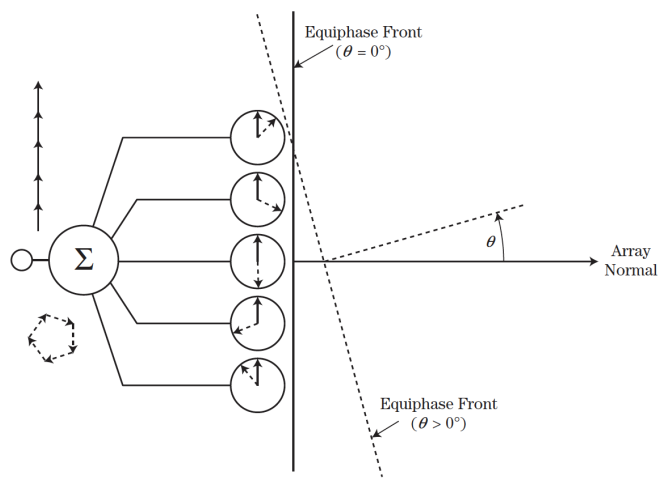

Figure 1.4: Constructive and destructive combination of wavefronts at the summation point in radar antenna arrays [1].

from an angle θ_s, the phase at that element, relative to the first, will be $-(2\pi/\lambda)n\Delta x \sin\theta_s$. If the array elements are to coherently combine at this incidence angle, a phase shift must be designed for each element at the feed network that will cancel the phase caused by the

propagation delay. Therefore, the phase shift at element n must be

$$\phi_n = \frac{2\pi}{\lambda} n\dot{\Delta}x \sin\theta_s \tag{1.11}$$

The AF can then be expressed as

$$AF(\theta) = \frac{1}{N}\sum_{n=1}^{N} \exp[-j\frac{2\pi}{\lambda} n\Delta x(\sin\theta - \sin\theta_s)] \tag{1.12}$$

and the total antenna directivity pattern can be formulated as

$$E(\theta) = E_e(\theta)AF(\theta) = \frac{E_e(\theta)}{N}\sum_{n=1}^{N} \exp -j\frac{2\pi}{\lambda} n\Delta x(\sin\theta - \sin\theta_s)] \tag{1.13}$$

where $E_e(\theta)$ is the antenna directivity pattern [1]. The peak occurs at θ_s. A phase shifter, which can change the phase delay from pulse to pulse, is added to each element of the antenna array. This allows the antenna to be electronically steered in the desired angle. A common issue with the phase shifter is quantization error. The phase shifter can only resolve the closest possible approximation of the desired angle. These errors are typically modelled by random errors and tend to increase the sidelobe of a beam pattern. Although it is possible to increase the phase shifter resolution, there will also be an increase in insertion loss [1].

Phase shifters are also not typically suitable for wideband radar application because the required phase delay for a beam is frequency dependent. Wideband radars offer larger resolution required to resolve targets that are close together. For wideband waveforms, the phase shifter can only be accurate for one frequency within the spectrum [1]. When the waveform has extended bandwidth, the total antenna directivity pattern changes to

$$E(\theta,\lambda) = \frac{E_e(\theta,\lambda)}{N}\sum_{n=1}^{N} \exp[-j2\pi n\Delta x(\frac{\sin\theta}{\lambda} - \frac{\sin\theta_s}{\lambda_0})] \tag{1.14}$$

where λ is the wavelength of any spectral component of the waveform and λ_0 is the wavelength at the center frequency where the phase shifter setting is determined. When $\frac{\sin\theta}{\lambda} - \frac{\sin\theta_s}{\lambda_0}$, the argument of the exponential is zero. This equation shows that a small change in frequency causes the beam to be mispointed with an error or angular squint represented by

$$\Delta\theta = \frac{\Delta f}{f_0}\tan\theta_s \tag{1.15}$$

where Δf is the difference between the instantaneous frequency and the center frequency. This is illustrated in figure 1.5 where each spectral component of the waveform will be scanned into a different direction centered about θ_s [1]. One way to correct the problem of

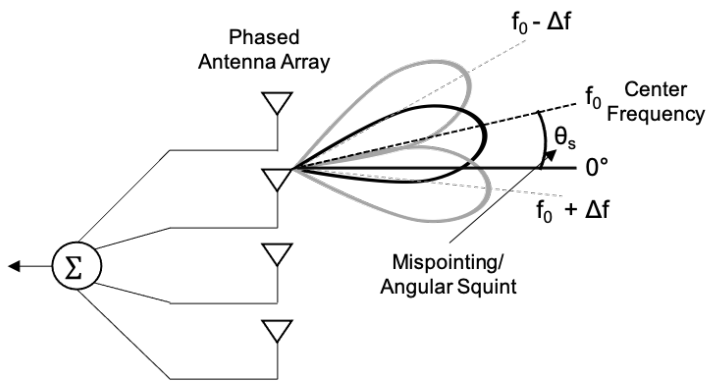

Figure 1.5: Mispointing error of Δf with wideband signals in phased array architectures [1].

phase shifters for wideband waveforms is using time delay units (TDUs). TDUs will adjust for the difference in arrival time for each element rather than the phase difference. All spectral components travel at the speed of light and have equal time delay thus eliminating the problem of beam squinting. However, TDUs are too large and costly to be used for each element in an antenna array. Another solution is utilizing subarray architecture. One possible solution to this is using a combination of phase shifters for each antenna and applying a TDU to a subarray rather than each element. The total directivity pattern of the TDU subarrayed architecture is

$$E(\theta,\lambda) = \frac{E_e(\theta,\lambda)}{MN} \tag{1.16}$$

$$= \frac{E_e(\theta)}{N}\sum_{n=1}^{N}\exp[-j\frac{2\pi}{\lambda}n\Delta S(\sin\theta - \sin\theta_s)]\sum_{n=1}^{N}\exp[-j\frac{2\pi}{\lambda}n\Delta x(\frac{\sin\theta}{\lambda} - \frac{\sin\theta_s}{\lambda_0})] \tag{1.17}$$

where M is the total number of subarrays and the subarray spacing is ΔS.

1.2.2 Digital Radar Architecture: MIMO Radar

MIMO or multiple-input multiple-output radars utilize multiple transmit and receive elements which emit and process independent waveforms, which unlike phased array antennas, are uncorrelated or orthogonal [5]. Waveforms are said to be orthogonal if

$$\int_{-\infty}^{+\infty} \phi_1(t)\phi_2^*(t)dt = 0 \tag{1.18}$$

The idea of MIMO started in communications where MIMO channels were used for a degree-of-freedom gain. The degrees of freedom allow for the spatial multiplexing of several data streams onto the MIMO channel. This results in an increase of capacity. Given a rich scattering environment, antennas that are not far apart will still allow the spatial separation of signals from different users [6].

The MIMO radar can be seen as an extension of phased array antenna systems, where instead of each element emitting a correlated signal with a different phase, MIMO radars need not be correlated. MIMO arrays are used to provide higher resolution, better sensitivity in detecting slow moving targets, better parameter identifiability, and direct applicability of adaptive array techniques [7]. MIMO radars have waveform diversity, which allows increased flexibility at the transmitter and allow probing signals to approximate a desired transmit beampattern that will minimize cross-correlation. MIMO allows for both transmit and receive digital beamforming and can utilize orthogonal waveforms which preserve the transmit degrees of freedom and improve the maximum number of resolvable targets. The M transmitting antennas increases the aperture length up to M times more than the receive array, achieving an M-fold improvement in the spatial imaging resolution over the conventional phased array [8].

MIMO radars can be categorized into two types: statistical MIMO and coherent MIMO. Statistical MIMO is the case where the elements are widely separated, similar to the traditional bistatic radar. It exploits the variation in spatial distance to improve detection and estimation performance. Coherent MIMO radars have transmit and receive elements closely

spaced, so the returns of a target are correlated from element to element where coherent processing can easily be applied [5].

The MIMO radar is able to synthesize a M times larger array, which results in a virtually larger antenna. If there are M transmit elements and N receive elements, the virtual array is described by the positions

$$\frac{\boldsymbol{x}_{T,m} + \boldsymbol{x}_{R,n}}{2} \tag{1.19}$$

where $\boldsymbol{x}_T$ and $\boldsymbol{x}_R$ are the positions of the transmit and receive elements respectively, $m = 1, \ldots, M$, and $n = 1, \ldots, N$. M transmitters emitting orthogonal waveforms with N receive elements will result in MN virtual phase centers which need not be distinct. By using a matched filter, the receiver will be able to detect the contribution from each transmitter [5].

For an angle of interest, θ, and specific wavelength, the transmit and receive steering vectors are defined as $\boldsymbol{a}(\theta)$ and $\boldsymbol{b}(\theta)$, respectively. When transmitting narrowband, nondispersive probing signals, the baseband signal at the target can be described as

$$\sum_{m=1}^{M_t} e^{j2\pi f_0 \tau_m(\theta)} x_m(n) \triangleq \boldsymbol{a}^*(\theta)\boldsymbol{x}(n) \tag{1.20}$$

where $n = 1, ..., N$, f_0 is the carrier frequency of the radar, τ_m is the time of travel between the mth transmit antenna and the target, N is the number of samples of each transmitted signal pulse, $\boldsymbol{x}(n)$ and $\boldsymbol{a}(\theta)$ is expressed as

$$\boldsymbol{x}(n) = \begin{bmatrix} x_1(n) & x_2(n) & \ldots & x_{M_t}(n) \end{bmatrix}^T \tag{1.21}$$

$$\boldsymbol{a}(\theta) = \begin{bmatrix} e^{j2\pi f_0 \tau_1(\theta)} & e^{j2\pi f_0 \tau_2(\theta)} & \ldots & e^{j2\pi f_0 \tau_{m_t}(\theta)} \end{bmatrix}^T \tag{1.22}$$

We let $y_m(n)$ be the received signal by the mth antenna, and define vectors $\boldsymbol{y}(n)$ and $\boldsymbol{b}(\theta)$ be defined as

$$\boldsymbol{y}(n) = \begin{bmatrix} y_1(n) & y_2(n) & \ldots & y_{M_r}(n) \end{bmatrix}^T \tag{1.23}$$

$$\boldsymbol{b}(\theta) = \begin{bmatrix} e^{j2\pi f_0 \tilde{\tau}_1(\theta)} & e^{j2\pi f_0 \tilde{\tau}_2(\theta)} & \dots & e^{j2\pi f_0 \tilde{\tau}_{m_t}(\theta)} \end{bmatrix}^T \tag{1.24}$$

where $\tilde{\tau}_m$ is the time needed by the signal reflected by the target to arrive at the mth receive antenna. The received data vector is

$$\boldsymbol{y}(n) = \sum_{k=1}^{K} \beta_k \boldsymbol{b}^*(\theta_k)\boldsymbol{a}^H(\theta_k)\boldsymbol{x}(n) + \boldsymbol{\epsilon} \tag{1.25}$$

The signal covariance matrix is defined as

$$\boldsymbol{R}_{\tilde{x}} = \frac{1}{N}\sum_{n=1}^{N} \tilde{\boldsymbol{x}}\tilde{\boldsymbol{x}}^* \tag{1.26}$$

Phased array is a special case of MIMO where each antenna element has a phase shifted version of the same signal. We can express the phased array signal as

$$x_{PA}(n) \triangleq \boldsymbol{a}^*(\tilde{\theta_0})x_0(t) \tag{1.27}$$

where $\boldsymbol{a}(\theta)$ is the transmit steering vector at angle θ, $\tilde{\theta_0}$ is the steering direction for each subarray, and $x_0(t)$ is the radar waveform. The signal correlation matrix is then expressed as

$$R_{x_{PA}} = \frac{1}{M}\boldsymbol{a}^*(\tilde{\theta_0})\boldsymbol{a}^*(\tilde{\theta_0})^H \tag{1.28}$$

If the emitted waveforms are orthogonal, the correlation matrix is full-rank and expressed as

$$R_{x/MIMO} = \frac{1}{M}\boldsymbol{I}_M \tag{1.29}$$

Assuming that the transmit and receive subarrays are identical, the two-way gain is expressed as

$$G(\theta;\theta_0) = \left(E_{TX}(\theta)\frac{|\boldsymbol{a}(\theta_0)^H\boldsymbol{R}_x^T\boldsymbol{a}(\theta_0)|^2}{\boldsymbol{a}(\theta_0)^H\boldsymbol{R}_x^T\boldsymbol{a}(\theta_0)}\right)\left(E_{RX}(\theta)\frac{|\boldsymbol{b}(\theta_0)^H\boldsymbol{b}(\theta)|^2}{N}\right) \tag{1.30}$$

where E_{TX} and E_{RX} are the one-way subarray gains for the transmit and receive elements. The gain equation shows that the transmit gain is heavily influenced by the signal correlation matrix [5].

1.2.3 Hybrid Radar Architecture: Phased-MIMO System

As mentioned previously, phased array radars are able to preserve the coherency of the signal which provides ease in processing return data. The more recent invention of MIMO radars tout waveform diversity as their strength. This allows reliable detection since it is much less likely for MIMO waveforms to simultaneously suffer from scintillation effects [9]. However, MIMO radars lose the transmit coherent processing gain that phased array radars benefit from, which leads to performance degradation and loss in SNR gain.

Using equation 1.30, the gain for the phased array and orthogonal waveforms can be formulated as

$$G_{PA}(\theta;\tilde{\theta}_0,\theta_0) = (E_{TX}(\theta)\frac{|\boldsymbol{a}(\tilde{\theta}_0)^H\boldsymbol{a}(\theta_0)|^2}{M})(E_{RX}(\theta)\frac{|\boldsymbol{b}(\theta_0)^H\boldsymbol{b}(\theta)|^2}{N}) \tag{1.31}$$

$$G_{MIMO}(\theta;\theta_0) = (E_{TX}(\theta)\frac{|\boldsymbol{a}(\theta_0)^H\boldsymbol{a}(\theta_0)|^2}{M^2})(E_{RX}(\theta)\frac{|\boldsymbol{b}(\theta_0)^H\boldsymbol{b}(\theta)|^2}{N}) \tag{1.32}$$

The phased array gain has a constant transmit steering angle of $\tilde{\theta}_0$, whereas the MIMO with orthogonal signals is able to change the steering angle θ_0 for the transmit beam [5].

The performance of an antenna array can be measured by using three gain patterns: the steered response, beam pattern, and point spread function (PSF). The steered response works to quantify how well the antenna array is able to steer itself in the desired direction. The beam pattern is used to measure the radar's ability to reject unwanted returns. The PSF helps to quantify the angular resolution.

One way to combine the benefits and mitigate the losses experienced with phased array and MIMO systems is utlizing subarrays. This method of utilizing subarrays is referred to as phased-MIMO [9] and is an example of a hybrid radar architecture where each subarray has specifically an orthogonal waveform. By partitioning the transmit array into subarrays, each subarray can transmit orthogonal waveforms, however, within the subarray, each element transmits coherent waveforms. Each subarray can have overlapping elements. Using this method, coherent processing gain can be achieved by designing the weights for the beam

for each subarray individually whilst keeping the upgraded resolution that MIMO provides the radar system. Additionally, this allows for adaptable beamforming techniques at the transmit and receive sides, offers robustness against interference, and provides a tradeoff between angular resolution and robustness against beam-shape loss [9]. A diagram of the phased-MIMO architecture is detailed in figure 1.6. The phased-MIMO radar beampattern

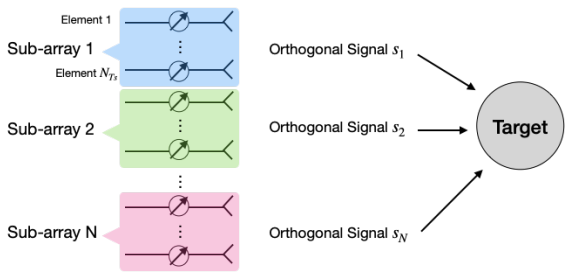

Figure 1.6: Phased-MIMO Diagram

can be written as

$$G_K(\theta) = \frac{|\boldsymbol{a}_K^H(\theta_s)\boldsymbol{a}_K(\theta)|^2}{(M-K+1)^2} \cdot \frac{|\boldsymbol{d}^H(\theta_s)\boldsymbol{d}(\theta)|^2}{K^2} \cdot \frac{|\boldsymbol{b}^H(\theta_s)\boldsymbol{b}(\theta)|^2}{N^2} \tag{1.33}$$

where $\boldsymbol{a}_K$ is the steering vector for the kth element, $\boldsymbol{d}$ is the K x 1 waveform diversity vector,

$$\boldsymbol{d}(\theta) = [e^{-j\tau_1}, \ldots, e^{-j\tau_K(\theta)}]^T \tag{1.34}$$

$\boldsymbol{c}$ is the transmit coherent processing vector,

$$\boldsymbol{c}(\theta) = [\boldsymbol{w}_1^H \boldsymbol{a}_1(\theta), \ldots, \boldsymbol{w}_K^H \boldsymbol{a}_K(\theta)]^T \tag{1.35}$$

M is the number of transmit antennas, and K is the number of subarrays. $\tau_k(\theta)$ is the time required for the wave to travel across the spatial displacement of the first antenna of the transmit array of the kth subarray. By defining $C_K(\theta) = \frac{|\boldsymbol{a}_K^H(\theta_s)\boldsymbol{a}_K(\theta)|^2}{(M-K+1)^2}$, $D_K(\theta) = \frac{|\boldsymbol{d}^H(\theta_s)\boldsymbol{d}(\theta)|^2}{K^2}$ and $R(\theta) = \frac{|\boldsymbol{b}^H(\theta_s)\boldsymbol{b}(\theta)|^2}{N^2}$, the phased-MIMO beampattern can be rewritten as

$$G_K(\theta) = C_K(\theta) \cdot D_K(\theta) \cdot R_K(\theta) \tag{1.36}$$

The phased array beam pattern can be found when $K = 1$ and the MIMO beampattern can be found when $K = M$. The phased-array and MIMO radar have the same overall

beampattern but they have different uplink and waveform diversity beampatterns as shown in figures 1.7 and 1.8. The phased-array radar has the highest possible transmit coherent

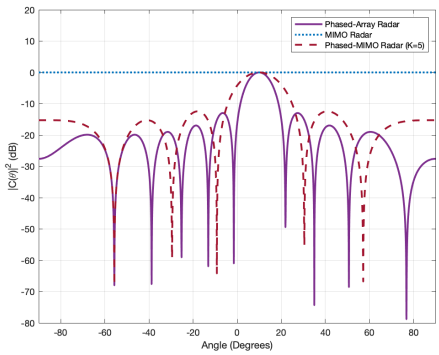

Figure 1.7: Transmit diversity gain for phased-MIMO.

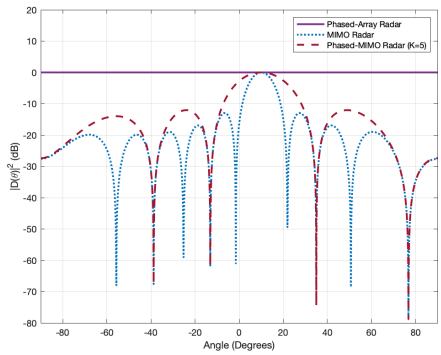

Figure 1.8: Waveform diversity gain for phased-MIMO.

processing gain but no diversity gain whereas the MIMO radar has the highest waveform diversity gain but no transmit coherent processing gain. A fully-overlapped phased-MIMO radar, where the subarray antenna elements overlap, is able to have the benefits of both since the overlapping of subarrays produces a narrower beam. The total beampattern is shown in figure 1.9. Using specialized beamformers such as the minimum variance distortionless

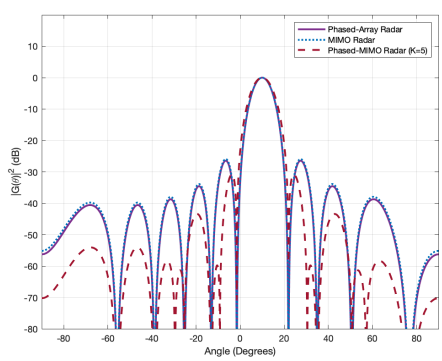

Figure 1.9: Total beampattern for phased-MIMO.

response (MVDR) and Capon beamformers used in [9] and [10] can further improve SNR performance.

1.3 Antenna Array Hardware Architectures

Phased array systems contain a number of antennas driven by circuitry that approximate relative time delays between antennas to steer toward a particular direction. The antennas are situated in a particular geometry in accordance to the application which helps to determine its array face. This is taken into consideration when beam steering. The beam is produced after the summation of all signals received by each antenna in the array. For a traditional phased array, the received signal undergoes beamforming which is made up of active, solid-state electronics, or passive splitting/combining and element-level electronics which are primarily analog [2].

An improvement on traditional analog phased arrays are hyrbid systems, such as the phased-MIMO, and fully-digital phased array systems. The hybrid system implements analog combining networks and phase shifters on particular antenna subarrays. The signals for each subarray are connected to digital beamformers that operate at the subarray level. This architecture helps to enable adaptive beamforming, space-time adaptive processing (STAP), and can handle multiple concurrent functions. Fully-digital phased array systems provide the most flexibility in terms of control of the signal and the ability to handle wideband signals. The digital system has an ADC and digital beamforming. This allows simultaneous beams and dynamic digital subarray allocation, adaptive digital beamforming, enhanced calibration for low sidelobes and wideband equalization, MIMO radar communication, and dynamic range improvements on the order of $10\log_{10}(N)$ dB where N is the number of transceivers [2]. These architectures can be summarized in figure 1.10.

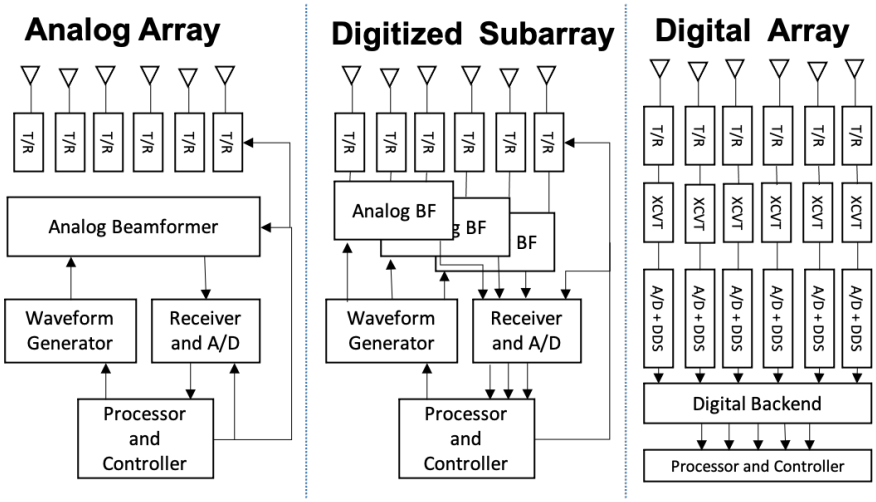

Figure 1.10: Analog, digitized subarray, and fully-digital antenna array architectures [2].

CHAPTER 2

Wideband Beamforming Algorithms

As stated before, there are problems that occur when using wideband signals. The beamforming algorithms that have been developed work only for narrowband systems and cannot carry over easily to wideband systems. Another problem is the beam squint or frequency invariance within the frequency band. There are several beamforming algorithms that can be implemented to help mitigate these problems. One algorithm, known as minimum variance distortionless response, or MVDR, is a common narrowband algorithm utilized for calculating sensor weights. A way to utilize this algorithm for wideband systems is by sub-banding. Sub-banding will essentially split the signal into several narrow sub-bands and the MVDR algorithm can be applied to each sub-band. An algorithm which helps with frequency invariance is the spatial response variation, or SRV, constraint method. This method constrains the fluctuation of the array beampattern over the desired frequency band by a small positive constant γ. This is an iterative optimization method.

The inverse discrete fourier transform method is a method that is implemented for rectangular antenna arrays. Utilizing the rectangular property, as well as a frequency transformation, we can use the 2-D inverse discrete fourier transform (2-D IDFT) to calculate real-valued antenna weights for each sensor. This method will be referred to as a frequency invariant beamforming, or FIB, processor. One issue with these algorithms is that they are not designed to maximize performance in terms of interference suppression. SINR, or signal to noise + interference ratio, is a metric used to measure the performance of wireless communications. In cases where it is vital to suppress interference at particular locations,

there needs to be a way to maximize this performance across the frequency band. Using P FIBs, we can additionally utilize the MVDR beamformer to generate P adaptive weights to generate a beamform that maximizes the SINR and improve the resolution. This section will expand on these established algorithms, some of which will be further implemented and analyzed.

2.1 Inverse Discrete Fourier Transform

The use of smart antenna arrays allows for better reduction of interference and increase in gain required for wideband systems [11]. Rectangular linear arrays are ideal for use with fully spatial signal processing with wideband systems because we can use the 2-D IDFT to calculate weights for each element [12]. We first define a uniform rectangular array, as shown in figure 2.1, of size M X N, with each element position as $(md_1,\ nd_2)$ where $m = \frac{-M-1}{2}, ..., \frac{M-1}{2}$, $n = \frac{-N-1}{2}, ..., \frac{N-1}{2}$, and d_1 and d_2 is the antenna element spacing for each direction. Each element has a corresponding weight $C_{m,n}$. An incoming signal $s(t)$ with

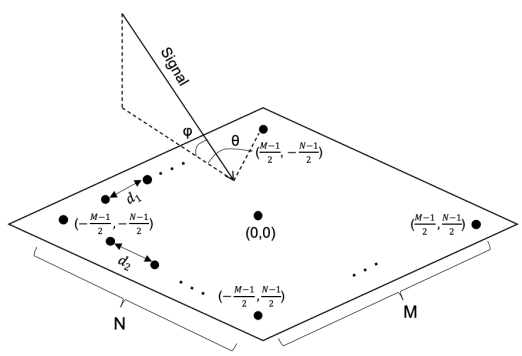

Figure 2.1: Planar Array Model

azimuth angle θ and elevation angle ϕ is processed at element (m, n) with sampling period T_s and represented in frequency domain via the 2-D DFT as

$$X_{m,n}(e^{j\omega}, \theta) = e^{j\frac{\hat{\omega}}{cT_s}(md_1 \sin\phi\cos\theta + nd_2 \sin\phi\sin\theta)} S(e^{j\omega}) \tag{2.1}$$

where c is the propagation velocity, $\hat{\omega} = \omega + 2\pi f_c T_s$, and f_c is the carrier frequency. Assuming the elevation angle is 90°, the beam pattern simplifies to

$$H(e^{j\omega}, \theta) = \sum_{\frac{-M-1}{2}}^{\frac{M-1}{2}} \sum_{\frac{-N-1}{2}}^{\frac{N-1}{2}} C_{m,n} e^{j\frac{\hat{\omega}}{cT_s}(md_1 \cos\theta + nd_2 \sin\theta)} \tag{2.2}$$

In order to create a frequency invariant beam pattern, we define a desired beam pattern $B(\theta)$ which is frequency invariant between $\omega_l \leq \omega \leq \omega_h$. This corresponds to the lowest and highest frequencies in $S(e^{j\omega})$. Using the transformations $\omega_1 = \hat{\omega}\frac{d_1}{cT_s}\cos\theta$, $\omega_2 = \hat{\omega}\frac{d_2}{cT_s}\sin\theta$, and $G(\omega_1, \omega_2) = H(e^{j\omega}, \theta)$, we can simplify to

$$G(\omega_1, \omega_2) = \sum_{\frac{-M-1}{2}}^{\frac{M-1}{2}} \sum_{\frac{-N-1}{2}}^{\frac{N-1}{2}} C_{m,n} e^{-jm\omega_1} e^{-jm\omega_2} = B(\tan^{-1}(\frac{\omega_2 d_1}{\omega_1 d_2}) \tag{2.3}$$

for $\frac{(cT_s)^2\omega_1^2}{d_1^2} + \frac{(cT_s)^2\omega_2^2}{d_2^2} \in [(\omega_l + 2\pi f_c T_s)^2, (\omega_h + 2\pi f_c T_s)^2]$. This resembles the Discrete Fourier Transform formulation. This means we can utilize the Inverse Discrete Fourier Transform to solve for the weights $C_{m,n}$, calculated as

$$C_{m,n} = \sum_{k=0}^{K-1} \sum_{l=0}^{L-1} G(\omega_1, \omega_2) e^{-jm\omega_{1k}} e^{-jm\omega_{2l}} \tag{2.4}$$

where $\omega_{1k} = -\pi + \frac{2\pi k}{K}$, $\omega_{2l} = -\pi + \frac{2\pi l}{L}$, $K = 2M$, and $L = 2N$ [11, 13]. This method of weight calculation will be referred to as Frequency Invariant Beamforming (FIB) processing. This algorithm can be summarized in figure 2.2.

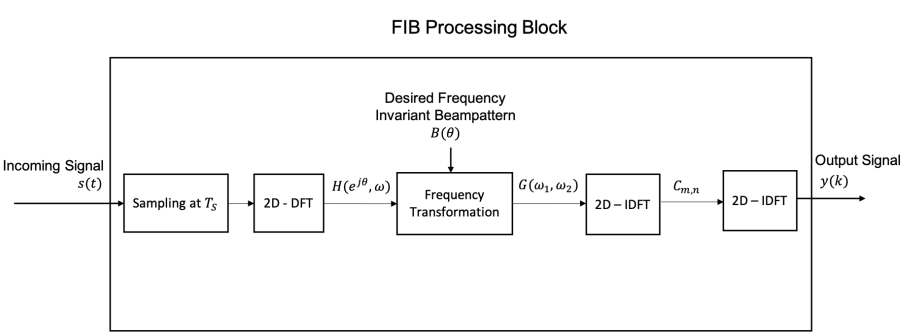

Figure 2.2: FIB Block Diagram

2.2 Frequency Invariance using SRV Constraint

The spatial response variation (SRV) is the measure of fluctuation of the array beampattern over the desired frequency band. It can be defined as

$$SRV(\theta) = \frac{1}{BW}\int_{f_l}^{f_h} |\boldsymbol{w}^T\boldsymbol{s}(f,\theta) - \boldsymbol{w}^T\boldsymbol{s}(f_0,\theta)|^2 df \tag{2.5}$$

where BW is the bandwidth of the signal, $\boldsymbol{w}$ is the real-valued weight vector, $s(f,\theta)$ is the spatial response, and f_0 is the frequency selected within the frequency range. The desired response of the beampattern is not fixed, but a function of the weight vector [14]. The SRV can be rewritten as

$$SRV(\theta) = \boldsymbol{w}^T\boldsymbol{C}(\theta)\boldsymbol{w} \tag{2.6}$$

where

$$\boldsymbol{C}(\theta) = \frac{1}{BW}\int_{f_l}^{f_h} [\boldsymbol{s}(f,\theta) - \boldsymbol{s}(f_0,\theta)]| \times [\boldsymbol{s}(f,\theta) - \boldsymbol{s}(f_0,\theta)]|^H df \tag{2.7}$$

Utilizing the fact that $\boldsymbol{C}(\theta)$ is a Hermitian matrix,

$$\boldsymbol{w}^T\boldsymbol{C}^H(\theta)\boldsymbol{w} = [\boldsymbol{w}^T\boldsymbol{C}^*(\theta)\boldsymbol{w}]^T = \boldsymbol{w}^T\boldsymbol{C}^*(\theta)\boldsymbol{w} \tag{2.8}$$

and

$$\boldsymbol{w}^T\boldsymbol{C}(\theta)\boldsymbol{w} = \boldsymbol{w}^T[\boldsymbol{C}(\theta) + \boldsymbol{C}^H]\boldsymbol{w}/2 = \boldsymbol{w}^T\boldsymbol{C}_r(\theta)\boldsymbol{w} \tag{2.9}$$

where $\boldsymbol{C}_r$ is the real part of $\boldsymbol{C}(\theta)$, $\boldsymbol{H}$ symbolizes the conjugate transpose, and $*$ symbolizes the conjugate. The SRV can be constrained by a small positive constant γ

$$\boldsymbol{w}^T\bar{C}_r\boldsymbol{w} \leq \gamma \tag{2.10}$$

where $\bar{C}_r$ is the average SRV, defined as

$$\bar{C}_r = \frac{1}{N}\sum_{i=1}^{N}\boldsymbol{C}_r(\theta_i) \tag{2.11}$$

This allows us to constrain the synthesized beampatterns at different frequencies to be similar. The SRV can be constrained in specified angles to be smaller than a specified threshold. The SRV constraint can also be designed for any direction of interest [14].

2.3 MVDR via Subbanding

The MVDR beamformer is only applicable for narrowband signals and will not work for wideband cases. One way to utilize MVDR beamforming for wideband signals is by subbanding. By using a frequency domain snapshot model, we can split the signal into multiple narrowband signals. This will allow us to find MVDR coefficients for each band. The DFT of the received signal at sensor n is

$$X_n\{m\} = \sum_{k=0}^{M-1} x_n(M-1-k)(e^{-j\frac{2\pi}{M}})^{km} \tag{2.12}$$

$$= x_n(M-1-k)(F_M)^{km} \tag{2.13}$$

where

$$F_m = e^{-j\frac{2\pi}{M}} \tag{2.14}$$

In matrix notation, it is represented as

$$\boldsymbol{X}_n = \boldsymbol{F}_M \boldsymbol{x}_n \tag{2.15}$$

where $\boldsymbol{X}_n$ represents the M frequency components at the output of sensor n. We process each of these vectors with a narrowband beamformer, such as the MVDR beamformer, to obtain M scalar outputs

$$Y\{m\} = \boldsymbol{w}^H\{m\}\boldsymbol{X}\{m\} \tag{2.16}$$

where the MVDR weights, $\boldsymbol{w}^H\{m\}$, are calculated as

$$\boldsymbol{w}^H\{m\} = \frac{\boldsymbol{v}_m^H \boldsymbol{S_X}^{-1}\{m\}}{\boldsymbol{v}_m^H \boldsymbol{S_X}^{-1}\{m\}\boldsymbol{v}_m} \tag{2.17}$$

The steering vectors are $\boldsymbol{v} = [\exp -2\pi f\tau_0, \exp -2\pi f\tau_2, \ldots, \exp -2\pi f\tau_{N-1}]$ where τ is the delay to the nth sensor, $f = f_c + m\Delta f$ for $m = 0, \ldots, \frac{M}{2} - 1$ and $f = f_c + (m-M)\Delta f$ for $m = \frac{M}{2}, \ldots, M-1$, and $\Delta f = \frac{1}{MT_s}$. The spatial spectral matrix is defined as

$$\boldsymbol{S}_X\{m\} = E[\boldsymbol{X}\{m\}\boldsymbol{X}^H\{m\}] \tag{2.18}$$

We can then sum the responses for each band to get the final output [15].

2.4 FIB Processing for MIMO Radars

There are also methods to create frequency invariant signals with fully digital MIMO arrays [11]. This method utilizes a MIMO antenna array with M transmitting antennas and N receiving antennas which are omnidirectional. The arrays are linear, colocated, and perpendicular to each other. The transmitted signal of the mth antenna is expressed as

$$s_m(t) = \tilde{s}(t)e^{j\Omega_m t} \tag{2.19}$$

where $\tilde{s}(t)$ is a wideband signal within the range f_l to f_h which constitutes bandwidth B. Ω_m follows

$$\Omega_{m+1} - \Omega_m \geq 2\pi B \tag{2.20}$$

where $m = 0, 1, ..., M-1$. This is so the transmitted signals are non-overlapping in frequency. The receiver has a bank of M linear phase filters that will separate the M transmitted signals. Each filter has a bandwidth of $2\pi B$, centered at Ω_m. The waveform incident on the target is

$$p(t) = \alpha \sum_{m=0}^{M-1} s_m(t - \frac{d}{c} m \sin\phi \cos\theta) \tag{2.21}$$

where α_1 is the attenuation factor, d is the antenna spacing, c is the propagation constant, ϕ is the elevation angle, and θ is the azimuth angle. The signal received at the nth antenna is

$$x_n(t) = \alpha_2 p(t - \frac{d}{c} \sin\phi \sin\theta) \tag{2.22}$$

for $n = 0, 1, ..., N-1$ where α_2 is the propagation attenuation. The target response is then expressed as

$$r_{n,m}(t) = \alpha s_m(t - \frac{d}{c}(m \sin\phi \cos\theta + n \sin\phi \sin\theta)) \tag{2.23}$$

where $\alpha = \alpha_1\alpha_2$. This can be summarized in figure 2.4. We assume the elevation angle is 90° and the response is sampled to get the frequency domain representation as

$$Y_{n,m}(e^{j\omega}, \theta) = \alpha e^{-j\frac{d}{cT_s}(\omega+\omega_m)(m\cos\theta + n\sin\theta)} \tilde{S}(e^{j\omega}) \tag{2.24}$$

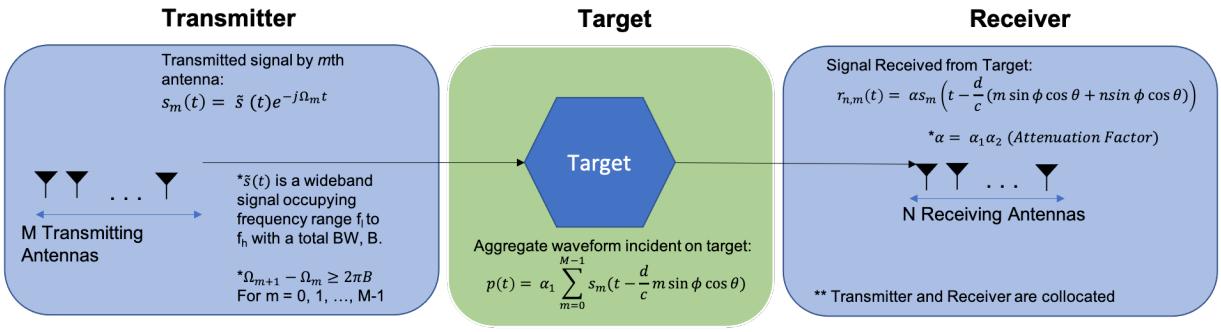

Figure 2.3: MIMO Radar Model Diagram

where $\omega_m = \Omega_m T_s$. Due to the addition of the $e^{-j\omega_m \frac{d}{cT_s}(m\cos\theta + n sin\theta)}$, it is not possible to perform IDFT to get proper weights. Instead, we use Least Squares approximation (LS). The output in frequency domain can be expressed as

$$Y(e^{j\omega}, \theta) = \alpha \sum_{m=0}^{M-1} \sum_{n=0}^{N-1} w_{n,m} e^{-j\frac{d}{cT_s}(\omega+\omega_m)(m\cos\theta + n\sin\theta)} \tilde{S}(e^{j\omega}) \tag{2.25}$$

and then we can define $G(\omega, \theta)$ as

$$G(\omega, \theta) = \sum_{m=0}^{M-1} \sum_{n=0}^{N-1} w_{n,m} e^{-j\frac{d}{cT_s}(\omega+\omega_m)(m\cos\theta + n\sin\theta)} \tag{2.26}$$

so that

$$Y(e^{j\omega}) = \alpha G(\omega, \theta) \tilde{S}(e^{j\omega}) \tag{2.27}$$

We sample $G(\omega, \theta)$ at M_1 frequency points between ω_l and ω_h. For each frequency point i, we sample $G(\omega_i, \theta)$ at N_1 angles between $\pi/2$ and $\pi/2$. We also sample $B(\theta)$, the desired frequency-independent beampattern at the same N_1 angles. In order to find the weights for each antenna element, we can set up a LS optimization problem

$$\min_{w_{n,m}} \quad \sum_{\omega_i} \sum_{\theta_k} |G(\omega_i, \theta_k) - B(\theta_k)|^2 \tag{2.28}$$

The closed-form solution is

$$\boldsymbol{w} = (\boldsymbol{A}^H \boldsymbol{A})^{-1} \boldsymbol{A}^H \boldsymbol{C} \tag{2.29}$$

where

$$\boldsymbol{w}_j = w_{n,m} \tag{2.30}$$

$$\boldsymbol{C}_i = B(\theta_{k_2}) \tag{2.31}$$

$$\boldsymbol{A}_{i,j} = e^{-j\frac{d}{cT_s}(\omega+\omega_m)(m\cos\theta_{k2}+n\sin\theta_{k2})} \tag{2.32}$$

The indices i and j are calculated as

$$i = k_1 N_1 + k_2, \qquad j = mN + n \tag{2.33}$$

with $m = 0, 1, ..., M-1$, $n = 0, 1, ..., N-1$, $k_1 = 0, 1, ..., M_1 - 1$, $k_2 = 0, 1, ..., N_1 - 1$. In the case where $\boldsymbol{A}$ is not full rank, we use the pseudo inverse of $\boldsymbol{A}$ [11]. The processing at the receiver can be summarized in figure 2.4.

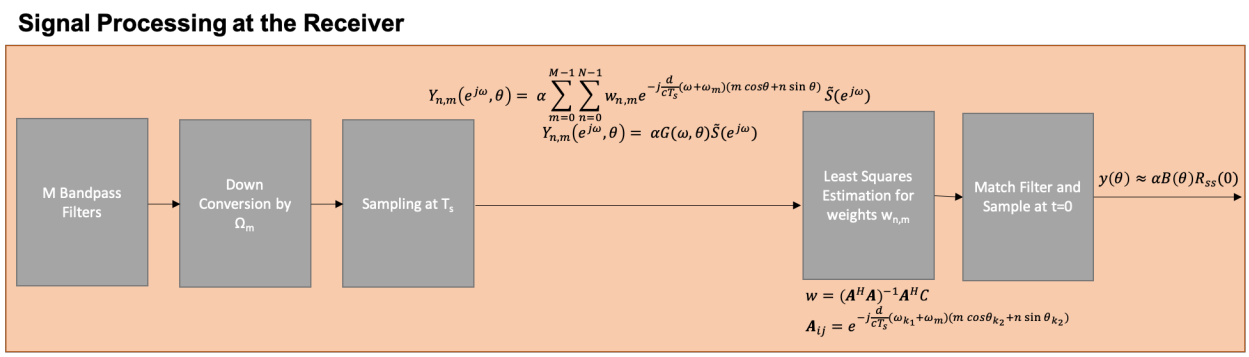

Figure 2.4: MIMO Radar Receiver Flow Diagram

2.5 FIB Processing with MVDR Beamforming

The FIB processing algorithm is not adaptive and does not maximize the gain or minimize specific noise or interference. We can utilize a performance metric, such as SINR, or the signal to noise + interference ratio, to assess the algorithm. A way to maximize the SINR and improve resolution of the beamformer is by adding MVDR beamforming. By passing the time-sampled input $x_{m,n}(k)$, where k is the time sample, into P FIB processors, we generate

P outputs. As mentioned before, the frequency invariant beamforming processors, or FIBs, are calculated via the IDFT method. The outputs, $y_p(k)$, are expressed as

$$y_p(k) = \sum_{i=0}^{I-1} B_p(\theta_i) s_i(k) + \eta_p(k) \tag{2.34}$$

where I is the number of incoming broadband signals, $B_p(\theta)$ is the desired beampattern, $s_i(k)$ is the ith incoming broadband signal incident on the array at θ_i $(i = 0, 1, ..., I-1)$, $s_0(k)$ is the desired signal, and η_p is the noise at the pth FIB. The pth FIB with constant weights $C^p_{m,n}$ form the pth beam as

$$\sum_{\frac{-M-1}{2}}^{\frac{M-1}{2}} \sum_{\frac{-N-1}{2}}^{\frac{N-1}{2}} C^p_{m,n} e^{-jm\omega_1} e^{-jm\omega_2} = B_p(\theta) \tag{2.35}$$

Each FIB output will be summed together after being multiplied by g_p where $p = 1, 2, ..., P$. These multipliers are calculated via the MVDR algorithm. We set $\boldsymbol{y} = [y_1(k), y_2(k), ..., y_p(k)]^T$ and $\boldsymbol{g} = [g_1(k), g_2(k), ..., g_p(k)]^H$ so the final output is

$$z(k) = \boldsymbol{g}^H \boldsymbol{y} \tag{2.36}$$

We can then formulate the optimization problem

$$\begin{aligned} \min_{g} \quad & \boldsymbol{g}^H \boldsymbol{R} \boldsymbol{g} \\ \text{s.t.} \quad & \boldsymbol{g}^H \boldsymbol{b} = 1 \end{aligned} \tag{2.37}$$

where $\boldsymbol{R} = E[\boldsymbol{y}\boldsymbol{y}^H]$ and $b = [B_1(\theta_0), B_2(\theta_0), ..., B_p(\theta_0)]^T$. The closed-form solution to the problem is expressed as

$$\boldsymbol{g} = \frac{\boldsymbol{R}^{-1}\boldsymbol{b}}{\boldsymbol{b}^H \boldsymbol{R}^{-1} \boldsymbol{b}} \tag{2.38}$$

This method will be able to suppress up to $P-1$ jammers and maximize SINR at the same time. The weights determined by the FIBs are all calculated offline which mean there is only P weights that need to be designed online [11].

CHAPTER 3

Hardware and Algorithm Considerations

Different architectures require different ways of mapping the algorithm onto hardware based on their constraints. Each architecture has its own degradation effects based on the hardware used. Analog systems, such as ones that use phased antenna arrays, depend on power amplifiers, attenuators, and phase shifters to be implemented. These components have negative effects on the resulting beampattern, such as phase shifter quantization. The resolution of phase shifters range from 2-6 bits which will effect the coefficient resolution for each algorithm. For digital systems, there are signal quantization effects resulting from the analog to digital converters. Digital systems also have coefficient quantization, but since the quantization is around bit-widths of 8-12, it not as pronounced as quantization resulting from phase shifters. Another implementation consideration for these algorithms is their computational complexity. Each mathematical operation results in more hardware and time to compute. This section will go over in detail the problems with associated hardware implementations as well as define the algorithm complexity used to evaluate algorithms.

3.1 Hardware Implementation

An important factor when considering algorithms is the associated performance degradation due to hardware quantization effects and component nonlinearities based on the chosen system architecture. Phased array systems have antenna elements with circuitry which depends on time delays to steer the element in a particular direction. The steering is controlled by the signal summation on the receiver or the radiation on the transmitter. Phased array systems

primarily use analog electronics. Hybrid systems utilize "digitized subarrays" where there is an analog combiner network as well as phase shifters and digital beamformers that accompany each subarray. This allows the use of adaptive beamforming. Fully digital systems utilize fully digital element-level processing and beamforming. These systems are touted to have more degrees of freedom to allow for more adaptive methods, enhanced calibration capabilities, MIMO communication, and dynamic range improvements. These systems require an Analog-Digital Converter and waveform generators on each element [2].

Phased array systems with analog beamforming use components such as amplifiers, attenuators, and phase shifters to obtain beamforming coefficients. Power amplifiers operate as linear devices under small-signal conditions but suffer from nonlinearities especially when dealing with higher, wideband frequency ranges. These nonlinearities include harmonic distortion, gain compression, inter-modulation distortion, phase distortion, adjacent channel interference, in-band signal distortion, and out-of-band spectral regrowth. In order to combat these nonlinearities, there are various linearization techniques that have been developed. An important tradeoff with power amplifier efficiency is that it often negatively impacts the device linearity which is important to consider when designing the system [16]. Components such as phase shifters cause arguably greater impact to the beampattern due to their limited resolution.

Phase shifters can be implemented in digital on a chip, or analog, but are still considered analog electronics. Analog phase shifters are most often controllled by voltage where as digital phase shifters, which are more commonly used, are controlled with digital bits. Digital phase shifters are not affected by noise on their voltage control lines. They have a discrete set of phase states that are controlled by two-state phase bits. For example, a 4-bit phase shifter has its highest order bit as 180°, continuing with 90°, 45°, and lastly, the least significant bit as 22.5°. Phase shifters are affected by inter-element spacing, physical size of the array, and resolution which can cause pulse distortion, inter-symbol interference, and beam squinting. Phase shifters typically follow low noise amplifiers in a receive array. The phase shifter's

insertion loss depends on the phase setting where its switching is represented by a finite time domain response. This has potential to cause bit error rate degradation [1, 17].

Digital systems are affected by both signal quantization and coefficient quantization. Due to the bit constraints imposed by the hardware such as an Analog-Digital Converter (ADC), the signals and filters are limited to a certain precision. One effect of this quantization is clipping of the signal. In the case when there is an ADC, the dynamic range of the ADC effects the maximum value, V_{ADC}, the signal can have. Any signal feature above the V_{ADC} is not detectable. Typically, the dynamic range is designed based on the expected dynamic range of the input signal. If the signal dynamic range is too large, receivers are accompanied with Automatic Gain Control which help to adjust to the signal power. Another source of quantization noise is the rounding of intermediate values. If dynamic range is fixed, the quantization noise is most effected by the number of bits used in calculations. Quantization error can be defined as

$$\epsilon_q = s(t) - s_q(t) \tag{3.1}$$

where ϵ_q is the quantization error, $s(t)$ is the original signal, and $s_q(t)$ is the quantized signal [16]. Along with signal quantization, there is additional effect of coefficient quantization. However, the coefficient quantization has minimal beampattern error relative to phase shifter errors.

System architectures are limited by the types of beamforming algorithms it can support. Each system has its own degradation effects and performance capabilities based on the effects of quantization discussed. The FIB processor can be implemented using either an analog or digital architecture as illustrated in figures 3.1 and 3.2. The analog diagram represents only coefficient quantization introduced by the phase shifter. The FIB + MVDR algorithm can be implemented as a fully-digital system or a hybrid system where the FIB coefficients are calculated in analog and the adaptable MVDR weights are calculated digitally. This digital and hybrid system is shown in figures 3.3 and 3.4. Lastly, the FIB processing for MIMO radars has to be done digitally.

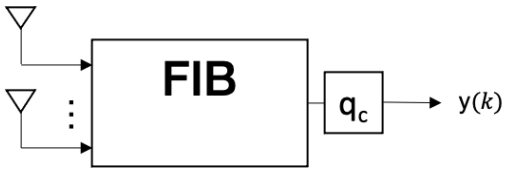

Figure 3.1: FIB processor for an analog system with coefficient quantization.

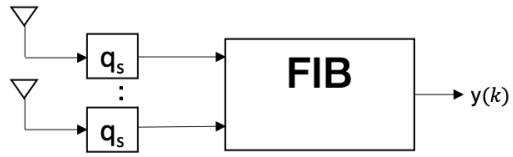

Figure 3.2: FIB processor for a digital system with ADC signal quantization.

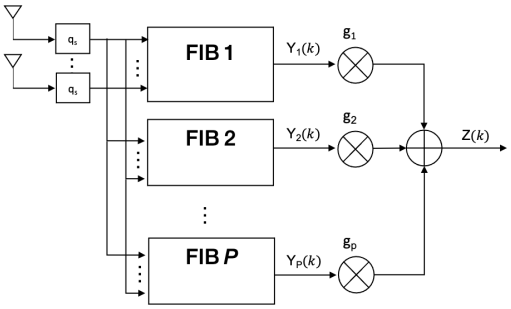

Figure 3.3: Block diagram for FIB + MVDR algorithm with digital system ADC effects.

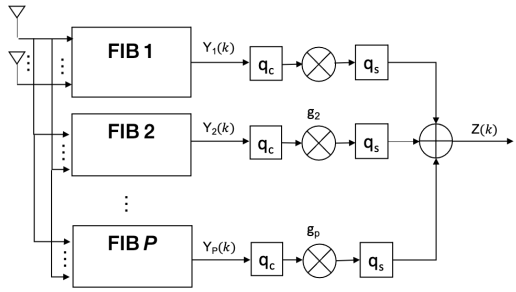

Figure 3.4: Block diagram for FIB + MVDR algorithm with hybrid system effects.

3.2 Computational Complexity

The computational complexity affects both time to execute and hardware required to implement algorithms, which is why it is pertinent when designing systems. When utilizing digital arrays, the number of floating point operations is what determines the computational complexity. Most adaptive beamforming algorithms, such as the MVDR beamformer, can be described with 4 essential steps: covariance matrix calculation, matrix inversion, weight computation, and application of weights to the data samples. When using N_c signals with N_s independent data support samples, the complexity for computing the covariance matrix is $8N_c^2N_s + 2N_c^2$ FLOPs. After the covariance matrix is calculated, it is then inverted where matrix inversion is N_c^3 FLOPs. The weight computation is $3N_c(N_c - 1)$ per beam. Finally,

the application of the weights to the signal is $8N_c^2(N_s - N_c/3) + 4PN_c^2$ for P beams. The FFT computation requires $5N_{ch}N_f \log N_f$ FLOPs, where N_{ch} is the number of digital channels, and N_f is the number of frequency bins [2]. The parameters are summarized in table 3.1.

Algorithm Complexity Parameters	
Parameter	Notation
Number of Signals	N_c
Degrees of Freedom	$N_d = N_c - 1$
Number of Signal Samples	N_s
Number of channels	N_{ch}
Number of Frequency Samples	N_f

Table 3.1: Summary of Algorithm Complexity Parameters

CHAPTER 4

Implementation and Evaluation

In this section, we will implement and analyze the IDFT or FIB processing algorithm, FIB + MVDR algorithm, and FIB for MIMO algorithm, using MATLAB software. We will evaluate the algorithms based on primarily their frequency invariance performance. For the FIB algorithm, we will test the performance of the algorithm against different desired beampatterns, that essentially have more null locations. For the FIB + MVDR algorithm, we evaluate the algorithm for 3, 7, and 11 FIB processors while also varying the interference angle direction. We also evaluate the algorithm performance with 2 interference directions, where one is fixed at 30° while the other is varied across the direction band. For the FIB for MIMO algorithm, we evaluate the performance across different frequency bands. Using the quantization effects described in the Hardware and Algorithm Considerations section, we implement and evaluate the FIB + MVDR algorithm performance with the quantization effects based on different bit-widths. This analysis will help understand both the benefits and shortcomings of these algorithms.

4.1 FIB Processing for Phased Array Radars

The constants and parameters used for the implementation of the FIB processing algorithm is summarized in table 4.1. The desired beampattern used for the implementation is

$$B_p(\theta) = \frac{1}{P}\frac{\sin(\frac{\pi P}{2}(\sin\theta - \frac{2p-P-1}{P}))}{\sin(\frac{\pi}{2}(\sin\theta - \frac{2p-P-1}{P}))} \tag{4.1}$$

FIB and FIB + MVDR Parameters		
Parameter	Notation	Value
Lower Frequency Band Edge	f_l	1.7 GHz
Upper Frequency Band Edge	f_h	2.7 GHz
Num. Antennas x Direction	M	17
Num. Antennas y Direction	N	17
Look Direction	θ_0	0°
Signal to Noise Ratio		40 dB
Interference to Noise Ratio		20 dB

Table 4.1: FIB and FIB + MVDR parameters and values used in implementation.

where P controls the number of nulls in the desired beampattern, and p controls the location of the main beam. The beampattern for the frequencies in the band of $1.7 - 2.7$ GHz for the case of $P = 3$ and $p = 2$ is shown in figures 4.1 and 4.2. The graphs show that there is no beam squint in the response. However, the depth of the nulls change throughout the frequency band. Figures 4.3 and 4.4 show the beampattern performance for when $P = 7$ and

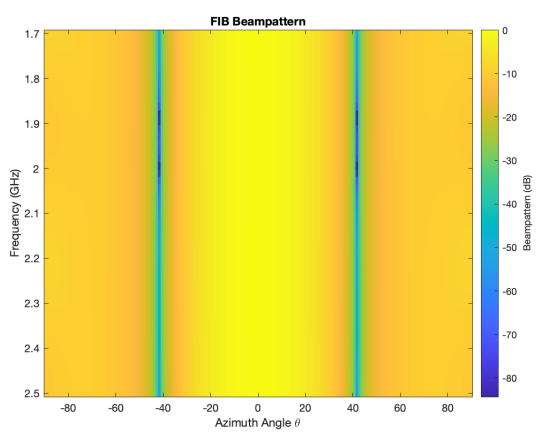

Figure 4.1: FIB Beampattern Spectrum Plot for P = 3

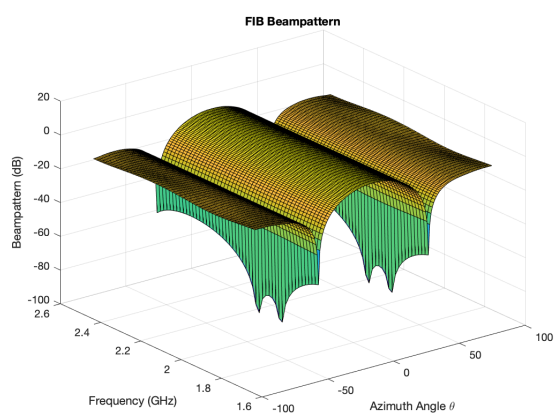

Figure 4.2: FIB Beampattern Surface Plot for P = 3

$p = 4$. The plots show a slight beam squint around $1.7 - 2$ GHz. The main lobe is mostly unaffected but the side lobes have a distinct curve. The depth of the null is also inconsistent across the frequency band. The null variation is more prominent towards the ends of the azimuth angle range. The squinting continues to become more severe as P increases, as seen

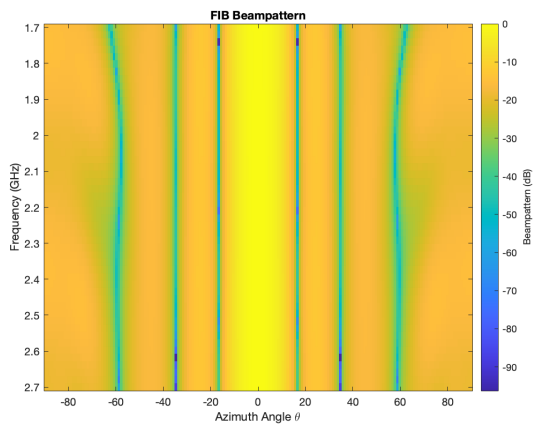

Figure 4.3: FIB Beampattern Spectrum Plot for P = 7

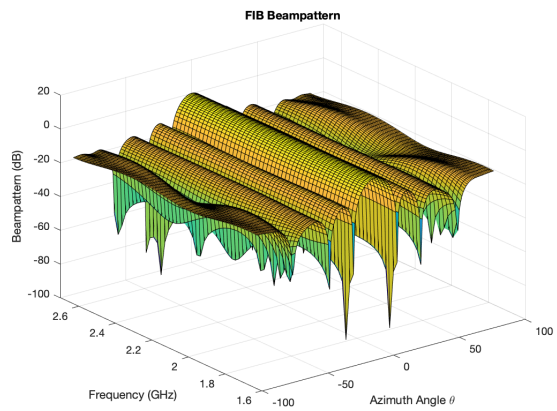

Figure 4.4: FIB Beampattern Surface Plot for P = 7

in figures 4.5 and 4.6 where $P = 11$ and $p = 6$. Again, the main lobe remains unaffected, but the ends of the beampattern have the most prominent beam squint. Tables 4.2 and 4.3 summarize the Mean Squared Error (MSE) across the frequency band and the azimuth angle range, respectively. The MSE values for $P = 7$ and $P = 11$ are relatively close, whereas the MSE values for $P = 3$ are much lower. This shows that the IDFT method produces coefficients that are much closer to the desired beampattern with fewer nulls. This is in part due to the desired beampattern being of a lower power level. If a desired beampattern with nulls that are not as deep was chosen, the error in response would decrease. The MSE for $P = 7$ is slightly larger than $P = 11$ because there happens to be more null variation for when $P = 7$.

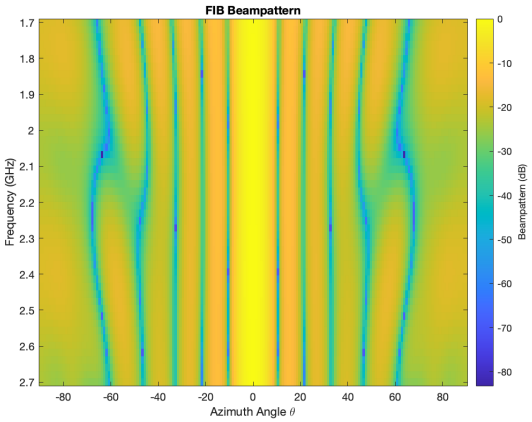

Figure 4.5: FIB Beampattern Spectrum Plot for P = 11

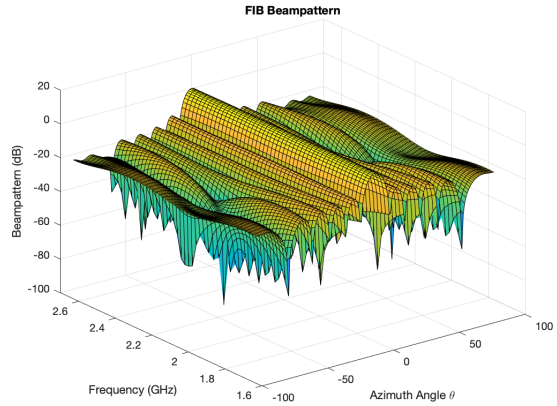

Figure 4.6: FIB Beampattern Surface Plot for P = 11

FIB MSE Performance Across the Bandwidth			
	Min. MSE	Max. MSE	Mean MSE
P = 3	1.81×10^{-7}	8.82×10^{-4}	3.47×10^{-4}
P = 7	7.87×10^{-1}	7.98×10^{-1}	7.92×10^{-1}
P = 11	4.98×10^{-1}	5.42×10^{-1}	5.18×10^{-1}

Table 4.2: Mean squared error across the frequency range.

FIB MSE Performance Across the Azimuth Angle Range			
	Min MSE.	Max MSE.	Mean MSE
P = 3	1.81×10^{-7}	8.82×10^{-4}	3.47×10^{-4}
P = 7	8.41×10^{-5}	3.41×10^{-1}	6.11×10^{-2}
P = 11	3.45×10^{-5}	3.42×10^{-1}	4.00×10^{-2}

Table 4.3: Mean squared error across azimuth angles.

4.2 FIB Processing with MVDR for Hybrid Radars

4.2.1 Sweeping the Interference Angle

For this implementation, each FIB uses the desired beampattern in equation 4.1, except each FIB has a different value of p from the range 1 to P. The MVDR algorithm will weight the coefficients derived from the IDFT for each FIB processor based on the angle of interference. The angle of interference is swept from $-\frac{\pi}{2}$ to $\frac{\pi}{2}$, excluding the angle of return signal which is set to $0°$. The total variance which the MVDR beamformer aims to minimize, is calculated for each angle of interference.

The first case is set to $P = 3$. Figure 4.7 shows the desired beampatterns for the 3 different FIB processors. Figure 4.9 shows the beampattern where the variance is the lowest and figure 4.10 shows the beampattern where the variance is the highest. Lastly, the variance as the interference angle location changes is shown in figure 4.8. The variances plotted on figure 4.8 correspond to the response at the lowest, middle, and highest frequency within the band, and also highlight the minimum, mean, and maximum variance throughout the entire frequency band. The variance increases drastically around $-20°$ to $20°$ so the highest variance is produced when the angle of interference is close to the look direction. The null is not constant within the frequency band, as the higher frequency beampattern shows the null about $20°$ away from the angle of interference. However, the variance for interferences not within $20°$ of the look direction is close to zero. The beampattern when the variance is low, as seen in figure 4.9, is consistent throughout the frequency band, and maintains the null throughout the angle of interference.

Figure 4.11 show the desired beampatterns for $P = 7$ FIB processors. The variances as the interference angle is swept throughout the angle range is shown in figure 4.12. We can see a dramatic difference in the width of the peak of highest variance relative to the variance graph in figure 4.8. The variance jumps to the peak variance at around $-8°$ to $8°$. With 7 FIBs, we are able to achieve frequency inavriant performance for more angles closer to the

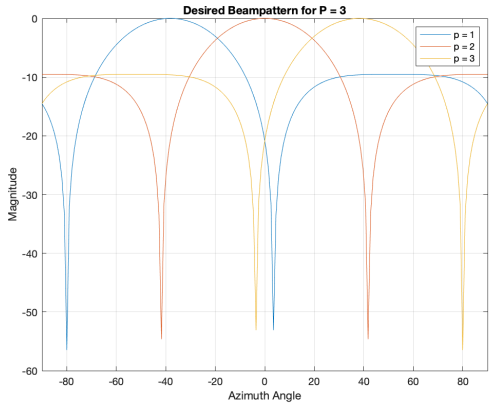

Figure 4.7: Desired beampatterns when P = 3.

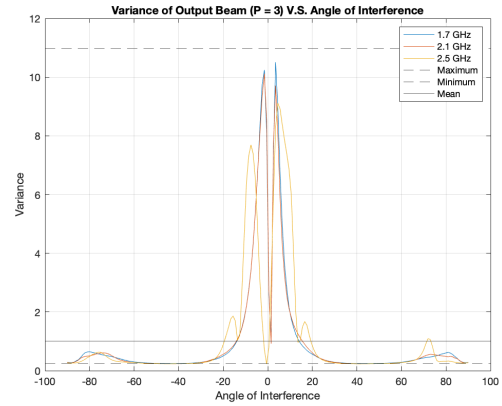

Figure 4.8: Variance for different interference angle locations when P = 3.

look direction. Figures 4.13 and 4.14 show the beampatterns for the angle of interference that produce the lowest and highest variance, respectively. It is apparent in these graphs that the ends of the beampattern are more frequency variant than the center.

Figure 4.15 shows the desired beampatterns for $P = 11$ FIB processors and figure 4.16 shows the variance for different interference angle locations. Figures 4.17 and 4.18 show the beampatterns for the angle of interference that produce the lowest and highest variance, respectively. The beampattern with the lowest variance shows a more frequency variant response compared to when $P = 3$. As P increases, the overall frequency invariance decreases, but, there is better precision in nulling the angle of interference. This can be further validated when introducing 2 interference angles. The number of FIB processors act as knobs that can be tuned to the chosen null location. The more knobs that are available allows us to have more control over said null location. However, a more complex desired beampattern with larger slopes and more changes throughout, is more difficult to replicate without error throughout the frequency band. The desired beampattern has a signifcant role in determining the frequency invariance and overall performance of the resulting beampattern.

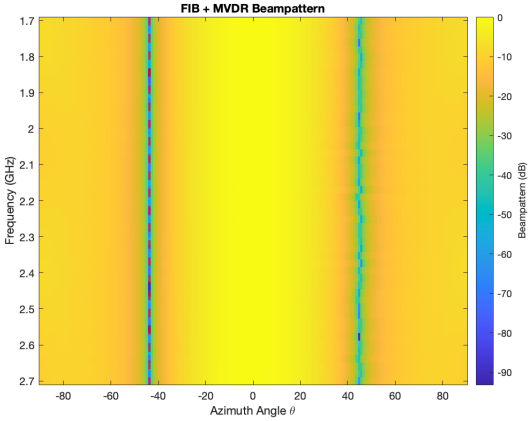

Figure 4.9: FIB beampattern with the lowest variance for P = 3.

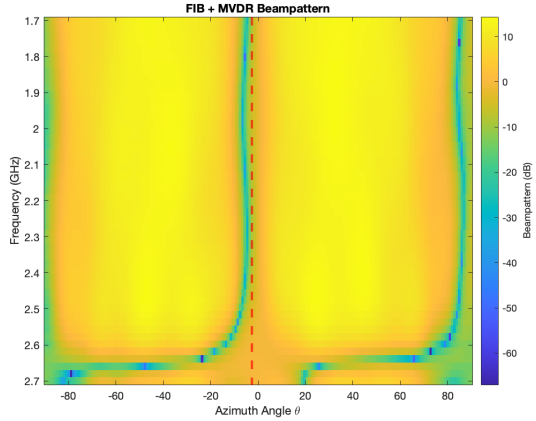

Figure 4.10: FIB Beampattern with the highest variance for P = 3.

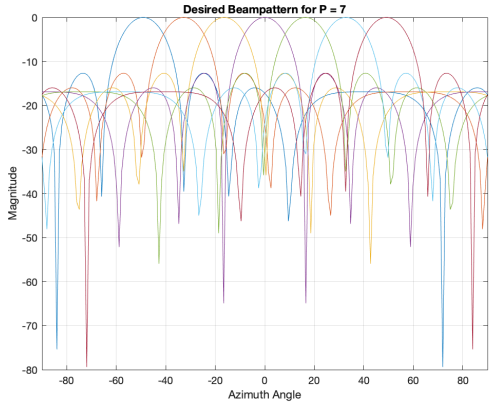

Figure 4.11: Desired beampatterns when P = 7.

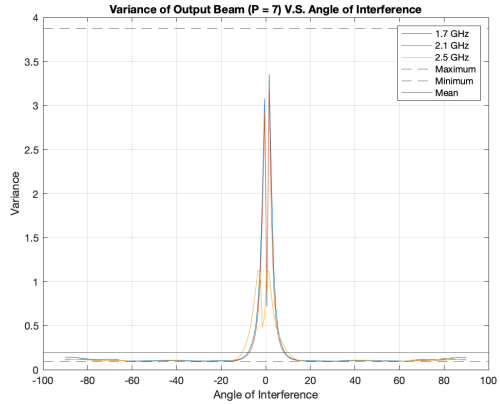

Figure 4.12: Variance for different interference angle locations when P = 7.

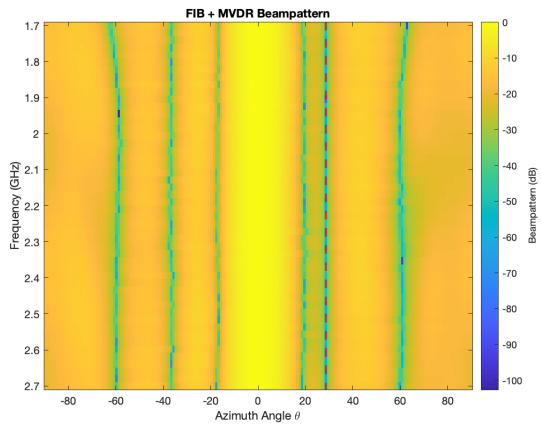

Figure 4.13: FIB beampattern with the lowest variance for P = 7.

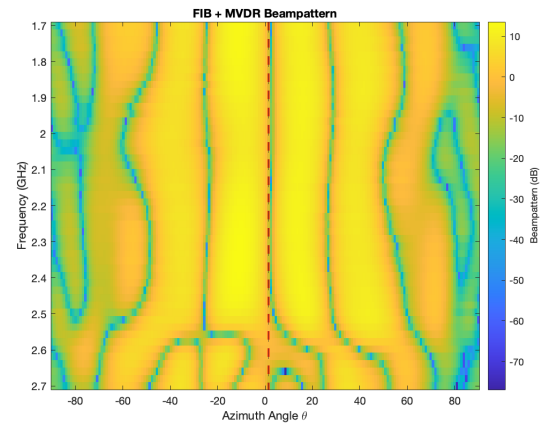

Figure 4.14: FIB beampattern with the highest variance for P = 7.

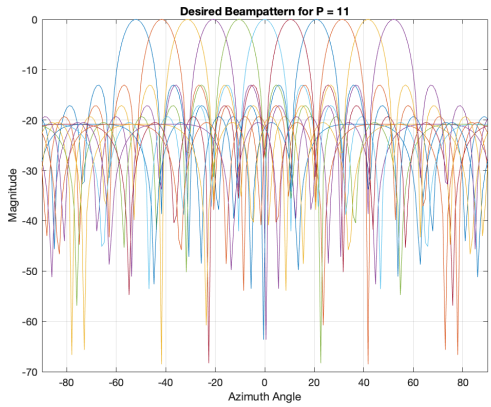

Figure 4.15: Desired beampatterns for P = 11.

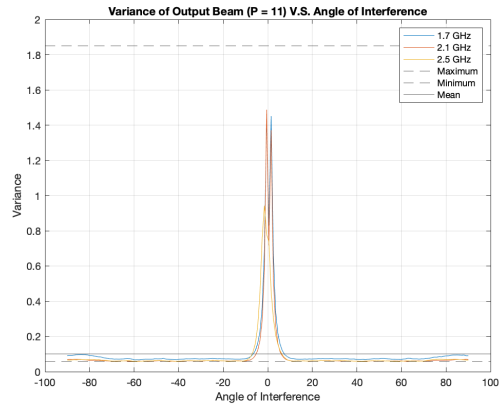

Figure 4.16: Variance for different interference angle locations when P = 11.

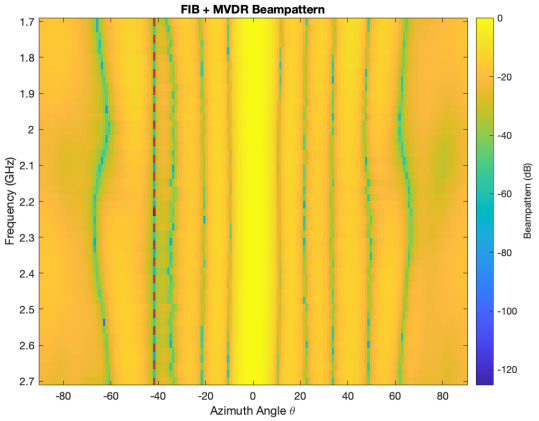

Figure 4.17: FIB beampattern with the lowest variance for P = 11.

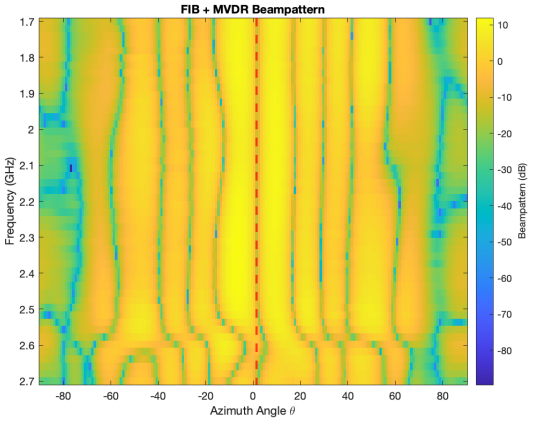

Figure 4.18: FIB beampattern with the highest variance for P = 11.

4.2.2 Performance for Two Interference Angles

For evaluating the performance of the FIB + MVDR algorithm with two interference angles, one interferer is kept constant at 30° while the other is swept across the $-\frac{\pi}{2}$ to $\frac{\pi}{2}$ range. The look direction is kept at 0°. Figures 4.19 and 4.20 are the beampatterns for the lowest and highest variance for $P = 3$ FIB processors. For two interferers, the lowest variance beampattern is not as consistent throughout the frequency band. Also, only one interference angle has a null, while the other is undetected. The beampattern for the highest variance occurs when the swept interferer is close to the look direction. Figures 4.21 and 4.22 are the

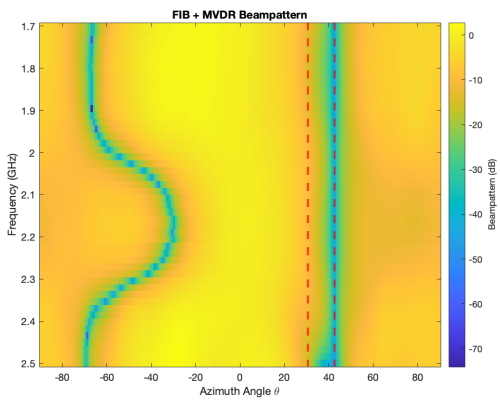

Figure 4.19: FIB+MVDR, Lowest Variance, 2 AOI, for P = 3

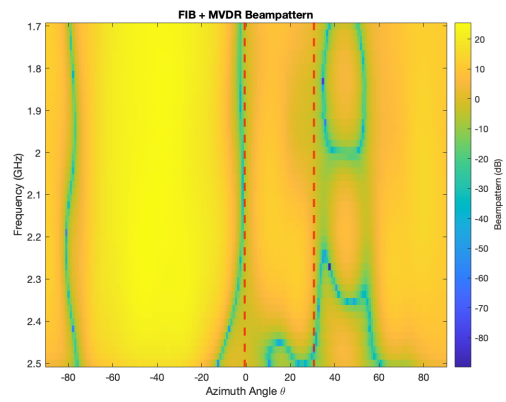

Figure 4.20: FIB+MVDR, Highest Variance, 2 AOI, for P = 3

beampatterns for the lowest and highest variance for $P = 7$ FIB processors. The performance for the beampattern with the lowest variance has nulls in the correct locations and the performance across the frequency band is relatively constant. Figures 4.23 and 4.24 are the beampatterns for the lowest and highest variance for $P = 11$ FIB processors. Similar to when $P = 7$, the performance for the beampattern with the lowest variance has nulls in the proper locations and the performance across the frequency band is also relatively constant.

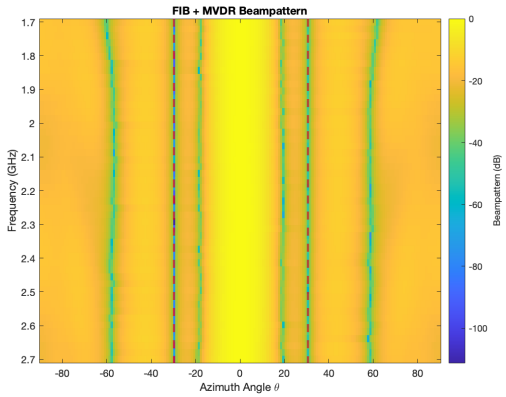

Figure 4.21: FIB+MVDR, Lowest Variance, 2 AOI, for P = 7

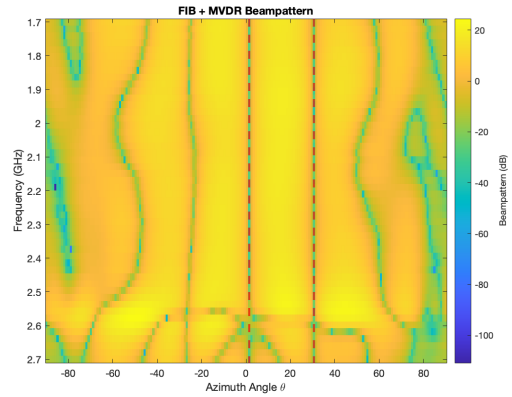

Figure 4.22: FIB+MVDR, Highest Variance, 2 AOI, for P = 7

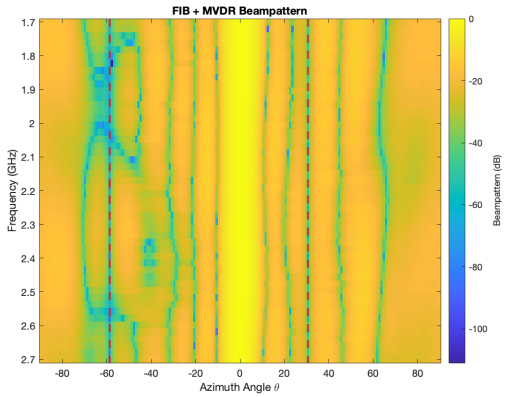

Figure 4.23: FIB+MVDR, Lowest Variance, 2 AOI, for P = 11

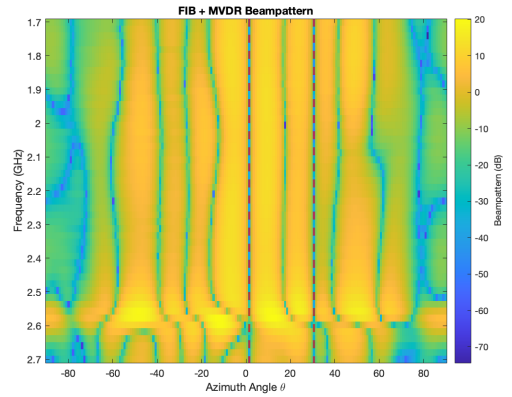

Figure 4.24: FIB+MVDR, Highest Variance, 2 AOI, for P = 11

4.3 FIB Processing for MIMO Digital Arrays

FIB for MIMO Parameters		
Parameter	Notation	Value
Num. Transmit Antennas	M	25
Num. Receive Antennas	N	25
Num. Carriers	Length of Ω_m	25
Num. Frequency Samples	M_1	50
Num. Angle Samples	N_1	180

Table 4.4: FIB for MIMO parameters and values used in implementation.

The FIB processor for MIMO digital arrays were evaluated for four different frequency bands: $1.7 - 2.7$ GHz, $3.2 - 5.1$ GHz, $21 - 33$ GHz, and $72 - 115$ GHz. The ranges were chosen so that the ratio of the bandwidth to the center frequency

$$FB = \frac{f_h - f_l}{\frac{f_h + f_l}{2}} \times 100\% \tag{4.2}$$

is the same at about 46%. The MIMO FIB beampattern across the frequency range is shown in in figures 4.25, 4.27, 4.29, and 4.31. The surface plot for the beampattern is shown in 4.26, 4.28, 4.30, and 4.32. As seen with the mean squared error across frequencies, shown in figure 4.36, and mean squared error across the angle range, shown in figure 4.35, the performance across different frequency bands is consistent. This is largely due to the fact that the ratio of the bandwidth to center frequency is the same for all chosen bandwidths. If a comparison between different ratios were done, the results would be more varied. The most significant error in terms of frequency is seen at the frequency band edges with a maximum mean squared error of about 4.4×10^{-4}. The most significant error in terms of the angle is at the center with a maximum mean squared error of 9.6×10^{-5}.

Figures 4.33 and 4.34 show the error between the desired beampattern and the beampattern calculated with the FIB using IDFT and FIB for MIMO algorithms, respectively.

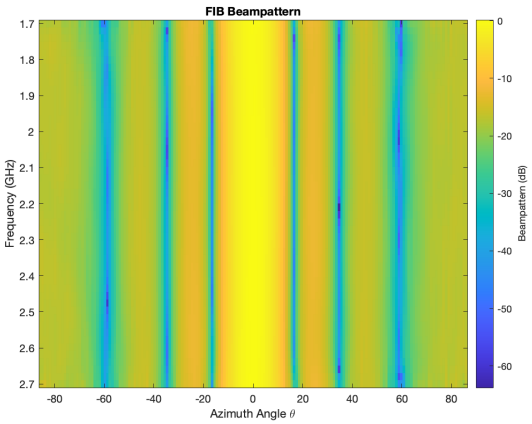

Figure 4.25: MIMO FIB beampattern for 1.7 - 2.7 GHz.

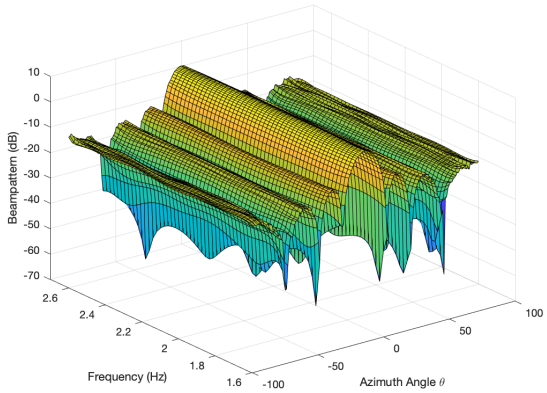

Figure 4.26: MIMO FIB beampattern surface plot for 1.7 - 2.7 GHz.

The FIB beampattern shows more error at the edges of the direction range. In general, the FIB beampattern is also more variant over the frequency band, regardless of the nulls being closer to the desired beampattern as seen with the large error spikes towards the beginning of the frequency band as well as the flattening of the beampattern across frequencies at its edges. This can also be seen with the nulls of main beam. The FIB for MIMO beampattern shows the mainbeam nulls having higher error than that of the FIB beampattern, however, there is decreased error at the peaks of the lobes.

MIMO FIB MSE Performance Across the Bandwidth			
	Min. MSE	Max. MSE	Mean MSE
1.7 - 2.7 GHz	5.149×10^{-5}	4.331×10^{-4}	8.847×10^{-5}
3.2 - 5.1 GHz	5.158×10^{-5}	4.331×10^{-4}	8.983×10^{-5}
21 - 33 GHz	4.043×10^{-5}	3.698×10^{-4}	7.601×10^{-5}
72 - 115 GHz	5.122×10^{-5}	4.362×10^{-4}	9.052×10^{-5}

Table 4.5: Mean squared error across the frequency range.

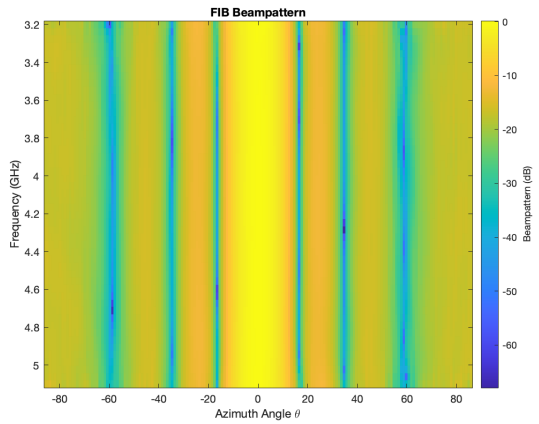

Figure 4.27: MIMO FIB beampattern for 3.2 - 5.1 GHz.

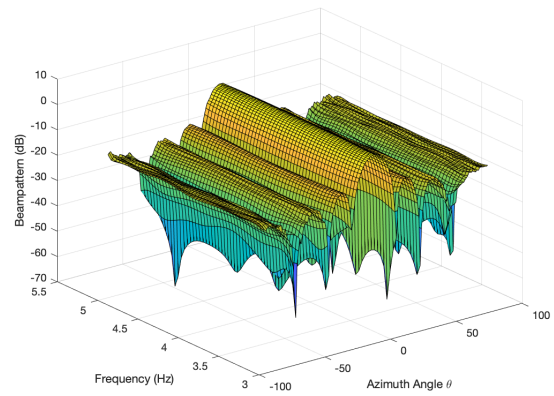

Figure 4.28: MIMO FIB beampattern surface plot for 3.2 - 5.1 GHz.

FIB MSE Performance Across the Azimuth Angle Range			
	Min MSE.	Max MSE.	Mean MSE
1.7 - 2.7 GHz	3.090×10^{-5}	9.598×10^{-5}	2.572×10^{-5}
3.2 - 5.1 GHz	5.188×10^{-6}	9.220×10^{-5}	2.611×10^{-5}
21 - 33 GHz	4.043×10^{-5}	4.194×10^{-6}	2.210×10^{-5}
72 - 115 GHz	4.521×10^{-6}	8.898×10^{-5}	2.631×10^{-5}

Table 4.6: Mean squared error across all azimuth angles.

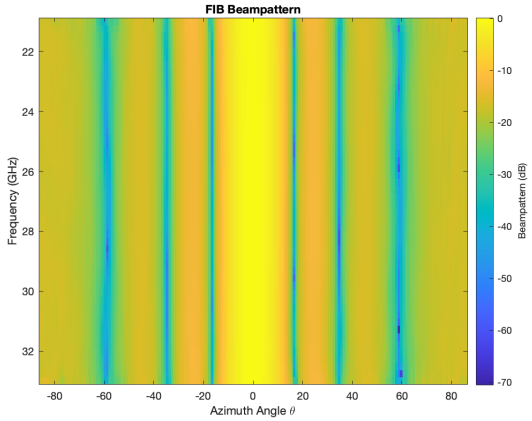

Figure 4.29: MIMO FIB beampattern for 21 - 33 GHz.

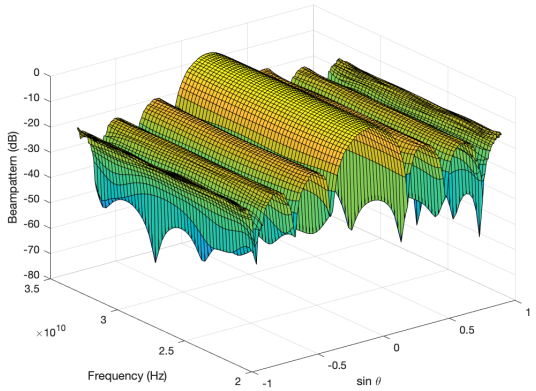

Figure 4.30: MIMO FIB beampattern surface plot for 21 - 33 GHz.

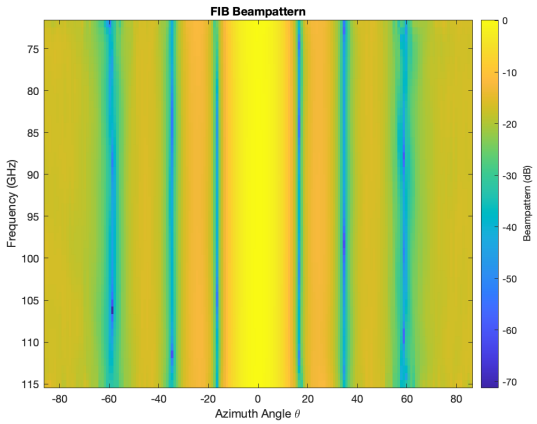

Figure 4.31: MIMO FIB beampattern for 72 - 115 GHz.

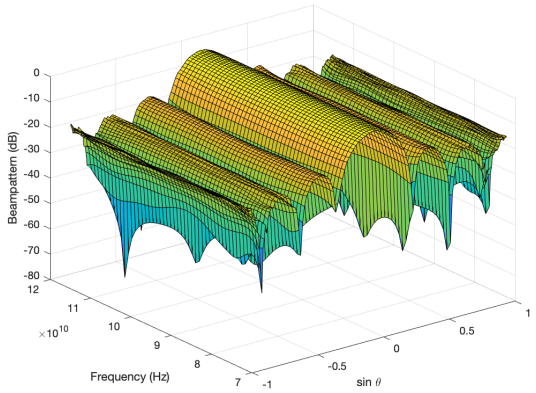

Figure 4.32: MIMO FIB beampattern surface plot for 72 - 115 GHz.

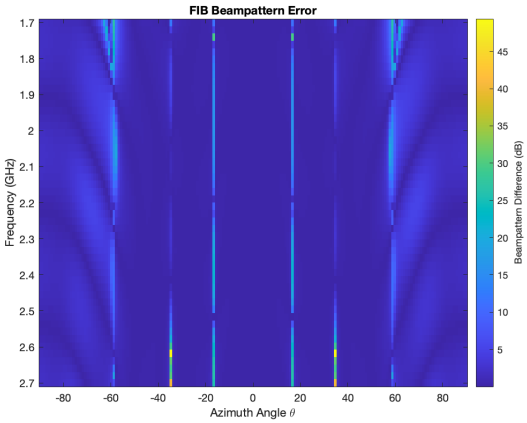

Figure 4.33: FIB Beampattern Error

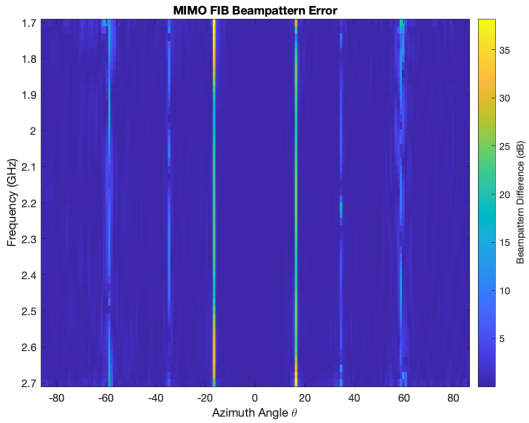

Figure 4.34: MIMO for FIB Beampattern Error

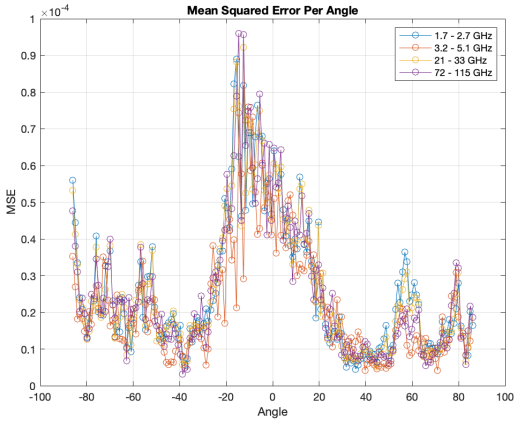

Figure 4.35: MIMO FIB Beampattern MSE across all angles.

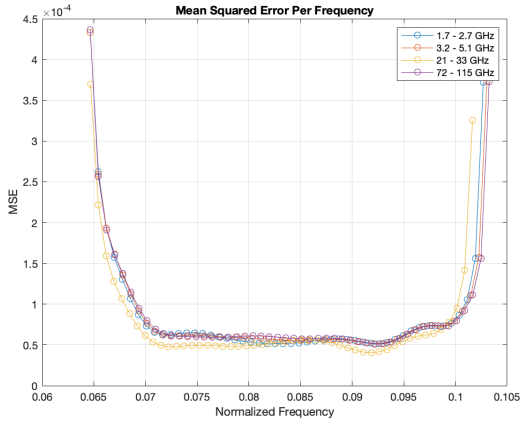

Figure 4.36: MIMO FIB beampattern MSE across the frequency band.

4.4 Hardware Analysis

The FIB + MVDR algorithm implemented with FIB coefficient quantization was tested for bit-wdiths 4, 6, 8, and 10 when $P = 3$. Typical phase shifter resolutions are 3-6 bits so we implement the beampatterns for 4 and 6-bits. To show the effects of larger bit-widths for a look into coefficient quantization for simple digital systems, 8 and 10 bit-widths were tested. The beam pattern for the lowest variance for all the bit-widths shown in figures 4.38, 4.40, 4.42, 4.44, successfully suppress the interference location across the frequency band. The 4 and 6 bit-widths show more frequency invariance across the bandwidth. When the bit-width reaches 10, the beampattern starts to resemble the beampattern without quantization shown in 4.9 and 4.10. The frequency invariance also improves significantly as the bit-width is increased. At lower bit-withds, the nulls of the beampattern change drastically within the frequency band. The results show that with an angle within the region where the variance is the highest, the beampattern suffers from the most frequency invariance. This is ultimately dependent on the number of FIBs used. The summary of performance can be seen in figures 4.45 and 4.46.

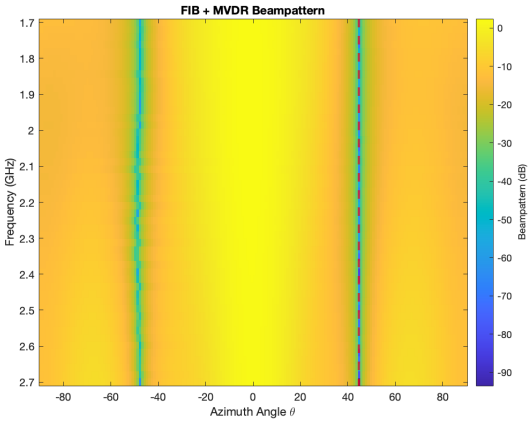

Figure 4.37: Quantized FIB+MVDR, Lowest Variance, bit-width = 4

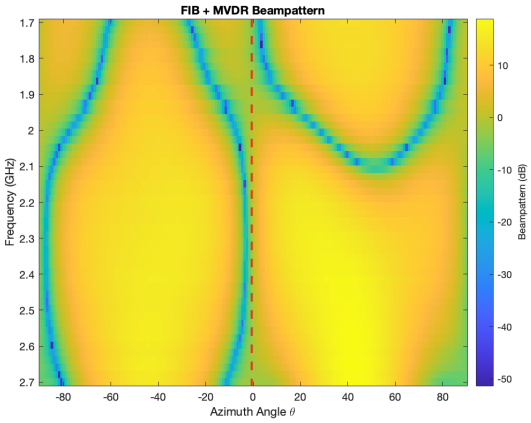

Figure 4.38: Quantized FIB+MVDR, Highest Variance, bit-width = 4

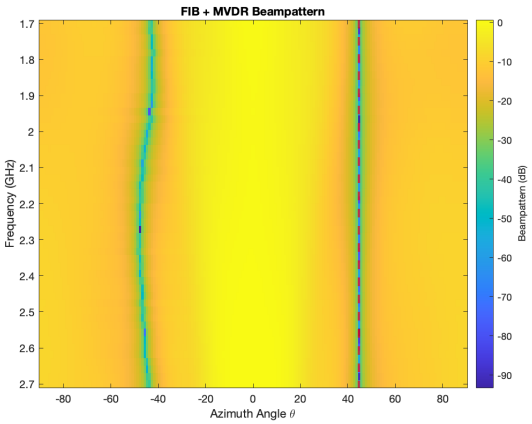

Figure 4.39: Quantized FIB+MVDR, Lowest Variance, bit-width = 6

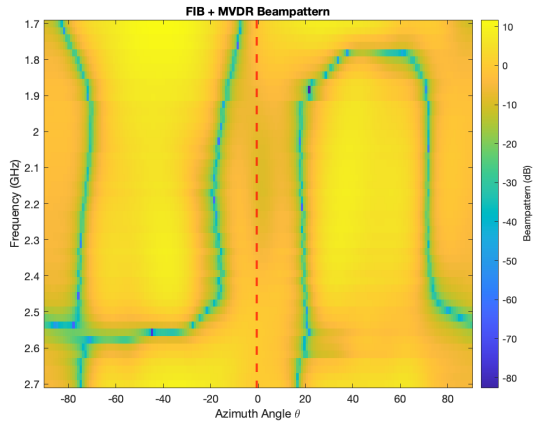

Figure 4.40: Quantized FIB+MVDR, Highest Variance, bit-width = 6

Along with quantization effects due to hardware, the computational complexity for the implemented algorithms were evaluated. The parameter definitions are summarized in table 3.1. The algorithm and associated complexity for each step is described in table 4.7, 4.8, and 4.9. For the FIB processor and FIB + MVDR algorithm, the number of channels would be equal to the number of antennas used which is 17x17. The number of frequency bins, N_f, is 50. The number of signals, N_c, is 1, and the number of samples of the signal, N_s, is $10,001$. For the FIB for MIMO algorithm, the number of channels would be equal to the

FIB Computational Complexity	
Technique	Complexity
2-D IDFT	$N_{ch} N_f \log N_f$
Application of Weights	$8N_c^2(N_s - \frac{N_c}{3}) + 4N_c^2$

Table 4.7: FIB Algorithm Computational Complexity

number of antennas used which is 25. The number of frequency bins, N_f, is 50, the number of angle samples, N_d, is 180, and the number of signals, N_c, is 1.

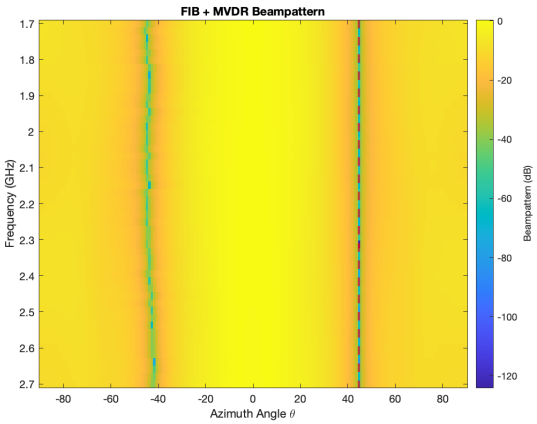

Figure 4.41: Quantized FIB+MVDR, Lowest Variance, bit-width = 8

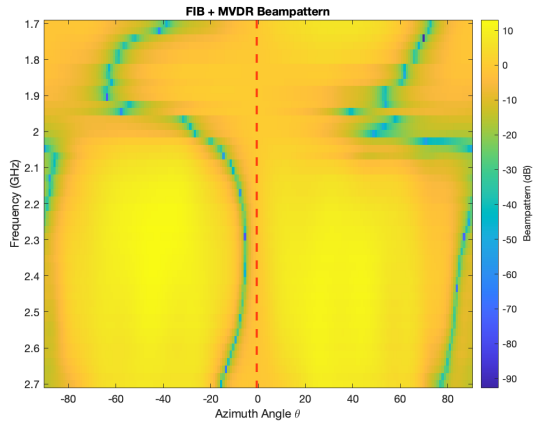

Figure 4.42: Quantized FIB+MVDR, Highest Variance, bit-width = 8

FIB + MVDR Algorithm Computational Complexity	
Technique	Complexity
2-D IDFT for each FIB	$N_{ch} N_f \log N_f$
Covariance Matrix	$8N_c^2 N_s + 2N_c^2$
Covariance Matrix Inversion	N_c^3
Compute Weights (MVDR)	$3N_c(N_c - 1)$ per beam
Application of Weights	$8N_c^2(N_s - \frac{N_c}{3}) + 4PN_c^2$ per beam

Table 4.8: FIB + MVDR Algorithm Computational Complexity

MIMO FIB Algorithm Computational Complexity	
Technique	Complexity
Matrix Inversion for LS	$N_f N_d N_{ch}^3$
LS Weight Calculation	$2N_f N_d N_{ch}$
Application of Weights	$8N_c^2(N_s - \frac{N_c}{3}) + 4N_c^2$

Table 4.9: MIMO FIB Algorithm Computational Complexity

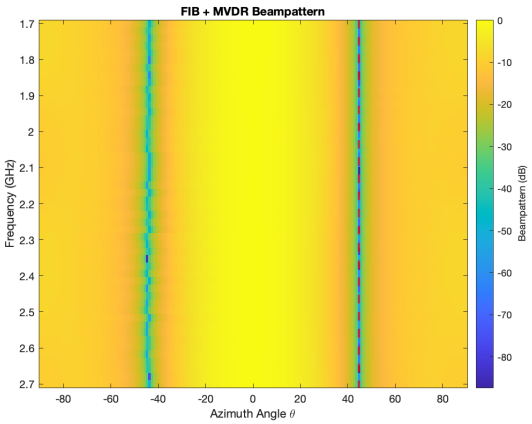

Figure 4.43: Quantized FIB+MVDR, Lowest Variance, bit-width = 10

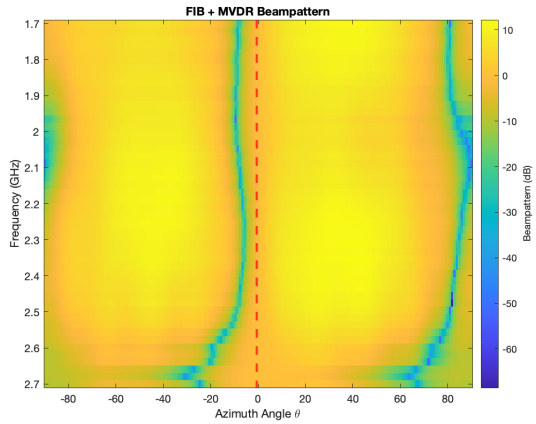

Figure 4.44: Quantized FIB+MVDR, Highest Variance, bit-width = 10

Summary of Algorithm Computational Complexity	
Algorithm	Calculated Complexity
FIB	$1.3346456e + 8$
FIB + MVDR	$1.0035339e + 12$
FIB for MIMO	$1.1390625e + 16$

Table 4.10: Summary of Algorithm Computational Complexity

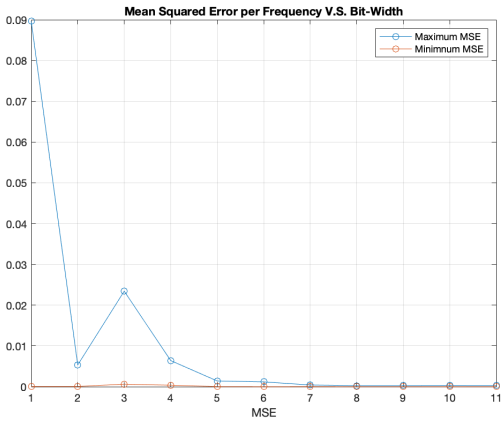

Figure 4.45: Quantized FIB+MVDR, MSE across Frequencies

Figure 4.46: Quantized FIB+MVDR, MSE across Angles

CHAPTER 5

Conclusion

In this thesis, we have detailed the issues associated with wideband radar systems and how they relate to analog, digital, and hybrid radar architectures. We have presented various wideband beamforming algorithms such as the Frequency Invariant Beamfoming processor (FIB) which utilizes the 2-D IDFT, the FIB + MVDR beamfomer, and the FIB for MIMO, that work to essentially achieve a frequency invariant response throughout the frequency band. Along with standard algorithm implementations, we also analyzed the effects of quantization due to the specific architecture as well as the the algorithm complexity based on the number of floating point operations, or FLOPs, required to implement in a digital system.

The FIB algorithm is able to create a frequency invariant response relatively close to the desired beampattern. However, there is increased frequency invariance shown as the desired beampattern becomes more complex. This means that its performance will vary depending on the desired beampattern. Another benefit of the FIB algorithm is that it generates real coefficients, meaning it can be easily implemented offline and in completely analog, hybrid or fully digital architectures. Since the FIB algorithm utilizes a desired beampattern, it is not adaptable. However, if it is combined with other adaptive algorithms, such as MVDR, it is able to null particular sources of interference. This is shown in the implementation of the FIB + MVDR algorithm. We can see more flexibility in nulling, especially when using a larger number of FIB processors to determine the MVDR coefficients.

The FIB + MVDR algorithm is able to work well for multiple interferers, depending

on the interferer location. As seen with the variance plots, interferers closer to the look direction will not be as frequency invariant as interferers further away from the look direction. Increasing the number of FIB processors used does help to mitigate that problem, but not completely. As P increases, the overall frequency invariance decreases, but, there is better precision in nulling the angle of interference. The FIB for MIMO algorithm works consistently well for more complex desired beampatterns and can be used in conjunction with adaptive algorithms, making it a viable digital algorithm.

The effects of coefficient quantization show how the lowest variance beampattern is relatively frequency invariant, but the highest variance beampattern has greater frequency variance. The nulls for the higher variance move drastically across the frequency band. As the bit-wdith increases to 10 bits, we can see the beampattern start to resemble the beampattern without quantization effects. This shows that digital systems with the ability to have larger bit-widths would not suffer as much from quantization effects as opposed to analog or hybrid systems.

Further research can go in various ways. One aspect that can be improved is the sidelobe suppression. Typically, we want the look direction to have the highest gain which means side lobes should have decreased prominence. There are ways to optimize sidelobe suppression that could be further implemented and analyzed. Another area of further work is looking at the performance for different interference signals. For this implementation, the interference was white noise. Having different interference signals would alter the way the FIB + MVDR algorithm performed. There can also be more attention to the waveform utilized with these algorithms. There are certain constraints for radar systems in terms of the transmitted waveform if these algorithms were implemented. We could also focus on analyzing further the hardware impacts to the beamforming performance. One example of this is to analyze the affects of utilizing non-ideal antennas. All implementations assumed omnidirectional antennas without accurate modeling of the antenna. Antennas come with their own signal degrading effects which can alter beampatterns and reduce performance.

References

[1] M. A. Richards, J. A. Scheer, and W. A. Holm, *Principles of Modern Radar: Basic Principles*. Institution of Engineering and Technology, 1 ed., 2010.

[2] C. Fulton, M. Yeary, D. Thompson, J. Lake, and A. Mitchell, "Digital phased arrays: Challenges and opportunities," *Proceedings of the IEEE*, vol. 104, no. 3, pp. 487–503, 2016.

[3] I. M. Skolnik, *Introduction to Radar Systems*. McGraw-Hill, 3 ed., 2001.

[4] B. Mahfahza and A. Elzerbani, *MATLAB Simulations for Radar Systems Design 1st Edition*. Chapman and Hall, 1st editio ed., 2003.

[5] M. A. Richards, J. A. Scheer, W. L. Melvin, and J. Scheer, *Principles of Modern Radar: Advanced Techniques, Volume 2*. Institution of Engineering and Technology, 2012.

[6] D. Tse and P. Viswanath, *Fundamentals of Wireless Communication*. Cambridge University, 2005.

[7] J. Li and P. Stoica, *MIMO Radar Signal Processing*. Wiliey-IEEE, 2008.

[8] W. Roberts, P. Stoica, J. Li, T. Yardibi, and F. A. Sadjadi, "Iterative adaptive approaches to MIMO radar imaging," *IEEE Journal on Selected Topics in Signal Processing*, vol. 4, no. 1, pp. 5–20, 2010.

[9] A. Hassanien and S. A. Vorobyov, "Phased-mimo radar: A tradeoff between phased-array and mimo radars," *IEEE Transactions on Signal Processing*, vol. 58, no. 6, pp. 3137–3151, 2010.

[10] D. Wilcox and M. Sellathurai, "On mimo radar subarrayed transmit beamforming," *IEEE Transactions on Signal Processing*, vol. 60, no. 4, pp. 2076–2081, 2012.

[11] P. Pal and P. P. Vaidyanathan, "Frequency invariant mvdr beamforming without filters and implementation using mimo radar," in *2009 IEEE International Conference on Acoustics, Speech and Signal Processing*, pp. 2081–2084, 2009.

[12] M. Ghavami, "Wideband smart antenna theory using rectangular array structures," *IEEE Transactions on Signal Processing*, vol. 50, no. 9, pp. 2143–2151, 2002.

[13] M. Uthansakul and M. Bialkowski, "Fully spatial wide-band beamforming using a rectangular array of planar monopoles," *IEEE Transactions on Antennas and Propagation*, vol. 54, no. 2, pp. 527–533, 2006.

[14] H. Duan, B. P. Ng, C. M. S. See, and J. Fang, "Applications of the srv constraint in broadband pattern synthesis," *Signal Processing*, vol. 88, no. 4, pp. 1035–1045, 2008.

[15] H. L. Van Trees, *Optimum Array Processing*. New York: Wiley-Interscience, 2002.

[16] R. Díez-García and A. Camps, "Impact of signal quantization on the performance of rfi mitigation algorithms," *Remote Sensing*, vol. 11, no. 17, 2019.

[17] R. R. Romanofsky, "Array phase phase shifters: Theory and technology," *National Aeronautics and Space Administration: Glenn Research Center*, 2007.